1   Supplement for "Large Contributions from Biogenic Monoterpenes and

2   Sesquiterpenes to Organic Aerosol in the Southeastern United States"

3

4   Lu Xu, Havala O.T. Pye, Jia He, Yunle Chen, Benjamin N. Murphy, Nga Lee Ng

5   correspondence to: ng@chbe.gatech.edu

6

7

8

S1. Experimental Procedure

The perturbation experiments were performed in July-August 2016. A 2m^3 Teflon chamber (cubic shape) (Fig. 1) was placed outdoor on the rooftop of the Environmental Science and Technology (ES&T) building on the Georgia Institute of Technology (GT) campus, which is 30-40m above the ground and 840m away from interstate I75/85. The eight corners of the chamber were open (~2"×2") to the atmosphere to allow for continuous exchange of air with the atmosphere. All analytical instruments were placed inside the building, which is about 4-5m away from the chamber. The instruments were connected to the chamber using 1/4" teflon tubings (for measurements of gas-phase species) or stainless steel tubings (for measurement of particle-phase species).

The perturbation procedure is described below and illustrated in Fig. A1. Firstly, we continuously flushed the chamber with ambient air using two fans, which were placed at two corners of the chamber. During this flushing period, all instruments sampled ambient air and were not connected to the chamber. The flushing period lasted at least 3 hours to ensure that the air composition in the chamber is the same as ambient composition. Secondly, we stopped both fans and connected all instruments to chamber. Due to particle waSll loss in the chamber, the particle mass concentration in the chamber was lower than that in the atmosphere (Fig. A1), but the particle composition in the chamber was almost the same as that in the atmosphere (Fig. S6), because the particle wall loss mainly depends on particle size not particle composition(Keywood et al., 2004). Due to the continued sampling by the instruments (~20 liter per minute, LPM) and the open corners of the chamber, ambient air continuously entered the chamber, even the two fans were turned off during this period. The main reason to turn off the fans is to increase the residence time of species in the chamber. The main reasons to leave the eight corners of chamber open are (a) to supply the chamber with atmospheric oxidants and (b) ensure that air composition in the chamber is representative of ambient composition. Thirdly, after sampling the chamber for about 30min, we injected certain amount of VOC (liquid) into the chamber with a needle, which vaporized upon injection. We continuously monitored the chamber composition for ~40 min after VOC injection. Lastly, we disconnected all instruments from the chamber, sampled ambient air, and turned on two fans to flush the chamber to prepare for the next perturbation experiment. In brief, one perturbation experiment can be divided into the following four periods: Amb_Bf (30min ambient measurement period before sampling chamber), Chamber_Bf (from sampling chamber to VOC injection, a

40   period ~30min), Chamber_Af (from VOC injection to stop sampling chamber, a period ~40min),

41   and Amb_Af (30min ambient measurement period after sampling chamber).

42   One to three experiments were performed per day. The interval between two experiments

43   was at least 3 hours, which avoids the interference of chamber content from previous experiments.

44   The perturbations were performed at different times of day to probe aerosol formation under

45   different reaction conditions. The injected amounts of α-pinene and β-caryophyllene were

46   carefully controlled to achieve an initial VOC concentration of about 14ppb and10ppb in the

47   chamber, respectively. If the injection amount is too large, it is not atmospherically relevant,

48   produces too much SOA, and biases the fate of organic peroxy radicals (RO_2), which may bias

49   subsequent analysis. If the injection amount is too small, the produced SOA would be too little

50   and below the detection limit of the experimental approach. The OA concentration in the chamber

51   after perturbation ranges from 4 to 16 $\mu g\ m^{-3}$, which is within the range of ambient OA

52   concentration. For isoprene and *m*-xylene perturbation experiments, we tried a range of initial

53   VOC concentrations (i.e., 10-90ppb for isoprene and 10-540ppb for *m*-xylene). For naphthalene

54   perturbation experiments, we injected naphthalene by passing pure air over solid naphthalene

55   flakes. We did not observe OA formation from these three VOCs, regardless of VOC concentration.

56   The possible reasons of the lack of OA formation will be discussed in section S6. Due to no OA

57   formation, the details about perturbation experiments with isoprene, *m*-xylene, and naphthalene

58   are not included in Table S4.

59   **S2. High Resolution Time-of-Flight Aerosol Mass Spectrometer (HR-ToF-AMS)**

60   The HR-ToF-AMS measures the chemical composition and size distribution of submicron

61   non-refractory species ($NR-PM_1$) with high temporal resolution. The details about HR-ToF-AMS

62   principles have been extensively discussed in the literature(Canagaratna et al., 2007; DeCarlo et

63   al., 2006). In brief, HR-ToF-AMS samples particles through an aerodynamic lens and then impacts

64   the particles on a ~600°C tungsten surface. Non-refractory species are flash evaporated and the

65   resultant vapors are ionized by 70eV electron impact ionization. The generated ions are analyzed

66   using time-of-flight mass spectrometry. In this study, the temporal resolution of HR-ToF-AMS

67   measurements was set to be 2 minutes and the instrument was only operated in V mode (resolving

68   power ~2100 at *m/z* 200). Ambient filter measurements (with a HEPA filter placed at the inlet of

69   sampling line) were performed periodically to eliminate gas-phase interference on the particle-

70   phase measurements by the HR-ToF-AMS. Ionization efficiency (IE) calibrations were conducted

71   every week with 300nm ammonium nitrate (AN) particles. A nafion dryer was placed upstream of

72   the HR-ToF-AMS to dry particles (relative humidity < 20%), which eliminated the potential effect

73   of relative humidity on particle collection efficiency (CE) at the HR-ToF-AMS vaporizer(Matthew

74   et al., 2008). The composition-dependent CE (i.e., CDCE) was applied to the data, based on the

75   algorithm proposed by Middlebrook et al.(Middlebrook et al., 2012) The elemental ratios, such as

76   atomic O:C and H:C, were calculated based on the method in Canagaratna et al.(Canagaratna et

77   al., 2015) The data analysis was performed using the standard AMS analysis toolkits SQUIRREL

78   v1.57H and PIKA v1.16H in Igor Pro 6.36 (WaveMetrics Inc.).

79   **S3. Positive Matrix Factorization (PMF) Analysis**

80   Positive Matrix Factorization (PMF) analysis has been widely used for aerosol source

81   apportionment in the atmospheric chemistry community(Jimenez et al., 2009; Crippa et al., 2014;

82   Xu et al., 2015a). PMF solves bilinear unmixing factor model(Paatero and Tapper, 1994; Ulbrich

83   et al., 2009b)

84                         $$X = TS \times MS + E$$ Eqn 2

85   X is an $m \times n$ matrix, representing m measurements over time of n species (i.e., m/z in AMS

86   measurements). TS is an $m \times p$ matrix, representing the factor strength (i.e., concentration in AMS

87   measurements) of the p factors. MS is an $p \times n$ matrix, representing the source profile (i.e., mass

88   spectra in AMS measurements) of the p factors. E is an $m \times n$ matrix, representing the unexplained

89   residual by the p factors. PMF solves the equation by minimizing the summed least squares errors

90   of the fit weighted with the error estimates of each measurement. In other words, PMF represents

91   the observed organic mass spectra as a linear combination of a number of factors with constant

92   mass spectra but varying concentrations over time. PMF groups OA constituents with similar mass

93   spectra and temporal variation into different factors, which are related to characteristic sources and

94   atmospheric processes.

95   In this study, we performed PMF analysis on the high-resolution mass spectra of organic

96   species (inorganic species are excluded) of combined ambient and perturbation data. Each OA

97   factor has a constant mass spectrum throughout the study, regardless of ambient or chamber

98   periods. The organic data matrix and error matrix were generated from PIKA v1.16H and

99　processed in the PMF Evaluation Toolkit (PET) software or Solution Finder (SoFi)
100　software(Ulbrich et al., 2009b). m/z's with signal-to-noise ratio between 0.2 and 2 were
101　downweighted by a factor of 2 to reduce disproportionate effects on the results(Ulbrich et al.,
102　2009a). We do not observe m/z's with signal-to-noise ratio smaller than 0.2. The errors of all CO_2^+
103　related peaks (i.e., O^+, HO^+, H_2O^+, CO^+, and CO_2^+) were downweighted, to avoid excessive
104　weighting of CO_2^+. The error of CHO^+ (m/z 29.0027) was downweighted by a factor of 2 as its
105　error appears to be underestimated, possibly due to interference from its adjacent N_2 isotope ion
106　(m/z 29.0032). We utilized the PMF2 solver, which does not require a priori information and
107　reduces subjectivity.

108　　　　Fig. 2 shows the time series and mass spectra of OA factors resolved in the measurements.
109　Five OA factors (i.e., HOA, COA, isoprene-OA, LO-OOA, and MO-OOA) are resolved. PMF
110　solutions with more than five OA factors display splitting behavior of existing factors instead of
111　providing new factors. Also, we note that PMF solutions with more OA factors cannot resolve one
112　factor that is capable of representing all perturbation induced SOA. The five identified OA factors
113　have been extensively discussed in previous studies (Xu et al., 2015a; Xu et al., 2015b; Xu et al.,
114　2017). Below, we will provide a brief but complete description about the unique features of these
115　OA factors.

116　　　　The mass spectrum of hydrocarbon-like OA (HOA) is dominated by hydrocarbon-like ions
117　($C_xH_y^+$ ions), which is similar to that of primary combustion emission species (Zhang et al., 2011).
118　The time series of HOA correlates well with primary emissions (i.e., black carbon and NO_x). Thus,
119　HOA is a surrogate of primary OA from vehicle emissions (Zhang et al., 2011).

120　　　　The mass spectrum of cooking OA (COA) is characterized by prominent signal at ions
121　$C_3H_5^+$ (m/z 41) and $C_4H_7^+$ (m/z 55), which is similar to the mass spectrum of unsaturated fatty acids
122　(Huang et al., 2010; Mohr et al., 2009). Cooking is an important source of primary emission in
123　urban sites(Xu et al., 2015a; Crippa et al., 2014; Huang et al., 2010), the concentration of which is
124　even higher than HOA concentration sometimes (Huang et al., 2010). We have clear evidence that
125　the COA factor at the measurement site has contributions from cooking activities. Firstly, the
126　diurnal variation of COA peaks during meal times (Fig. S3a). Secondly, in another dataset from
127　the same measurement site, the COA concentration shows clear increases on football days,
128　consistent with barbecue activities on campus and close to the measurement site. Thirdly,

129   compared to most of days during 2015 measurement (section S4), the COA concentration is higher

130   between August 13th and 16th, 2015 (Fig. S3b and S3c). These four days are right before the start

131   of a new semester and thus there are many fraternity rush events (i.e., barbecue activities) on

132   campus. However, the COA concentration increases in 5 out of 6 β-caryophyllene perturbation

133   experiments and its enhancement amount is ~25% of LO-OOA enhancement (Fig. S7b), which

134   demonstrate that COA factor could have interference from β-caryophyllene SOA. Thus, caution is

135   required when using COA factor as a surrogate for cooking emissions, especially for urban sites

136   influenced by air masses from forested areas.

137   Ample evidence suggests that the isoprene-derived OA (isoprene-OA) factor is related to

138   the reactive uptake of isoprene oxidation products, isoprene epoxydiols (IEPOX) (Xu et al., 2015a;

139   Lin et al., 2012; de Sá et al., 2016). Firstly, the mass spectrum of isoprene-OA is characterized by

140   prominent signal at ions C$_4$H$_5$$^+$ (*m/z* 53) and C$_5$H$_6$O$^+$ (*m/z* 82), which is similar to the mass spectrum

141   of laboratory IEPOX SOA (Lin et al., 2012). Secondly, the time series of this factor correlates well

142   with 2-methyltrols, which are tracers for isoprene SOA tracers and likely formed from the reactive

143   uptake of IEPOX. This factor is also referred to as "IEPOX-OA" in some studies (Hu et al., 2015;

144   Budisulistiorini et al., 2013; Budisulistiorini et al., 2015; de Sá et al., 2017).The isoprene-OA

145   factor contributes 18-36%, 34%, and 24% of OA in the southeastern U.S. (Xu et al., 2015a),

146   Amazonia forest (Chen et al., 2015), and boreal forest (Robinson et al., 2011). In our study,

147   isoprene-OA increases in 7 out of 19 α-pinene experiments and its enhancement magnitude is ~20%

148   of LO-OOA enhancement (Fig. S7a). Our results clearly demonstrate that the isoprene-OA factor

149   could have interferences from α-pinene SOA. Thus, this factor is neither exclusively from the

150   reactive uptake of IEPOX nor isoprene oxidation. This conclusion could be applicable to isoprene-

151   OA factor resolved at other monoterpene-influenced sites, but the interference magnitude likely

152   varies between sites. Considering that the isoprene-OA factor has the largest tendency to absorb

153   water and act as cloud condensation nuclei among all OA factors (Cerully et al., 2015), thorough

154   investigations on the sources of this factor are critical to accurately understand the climate forcing

155   of OA. From another aspect, the enhancement in isoprene-OA in these experiments suggests that

156   fresh α-pinene SOA is not exclusively apportioned to LO-OOA, at least for the sites with isoprene-

157   OA.

158   The isoprene-OA enhancement is not due to that the injected α-pinene affecting the

159   oxidation of pre-existing isoprene or the gas/particle partitioning of pre-existing semi-volatile

160   species in the chamber. After injecting α-pinene, the SOA concentration increases less than 3 µg

161   m^{-3}, which does not substantially perturb the gas/particle partition of pre-existing semi-volatile

162   species. Based on I$^-$ HR-ToF-CIMS measurement, the concentration of isoprene oxidation

163   products, such as IEPOX+ISOPOOH ($C_5H_{10}O_3 \cdot I^-$) and isoprene hydroxyl nitrates ($C_5H_9NO_4 \cdot I^-$),

164   did not change after α-pinene injection (Fig. S2b).

165   Less-oxidized oxygenated organic aerosol (LO-OOA) and more-oxidized oxygenated

166   organic aerosol (MO-OOA) are named based on their differing carbon oxidation state. MO-OOA

167   has the highest atomic O:C ratio, indicating that it is highly oxidized. LO-OOA has lower O:C

168   ratio than MO-OOA. In the southeastern U.S., MO-OOA concentration peaks in the afternoon and

169   LO-OOA exhibits a daily maximum at night (Xu et al., 2015b). The sources/processes contributing

170   to LO-OOA and MO-OOA are largely unknown. Based on the comparison with external

171   independent tracers and mass spectra of laboratory OA generated under various conditions,

172   previous studies proposed that LO-OOA represents fresh SOA, MO-OOA represents aged SOA,

173   and LO-OOA evolves to MO-OOA with photochemical aging (Jimenez et al., 2009; Ng et al.,

174   2010). Recent studies have advanced our understanding of these OA factors. For example, some

175   studies suggested that MO-OOA has contribution from aged biomass burning emissions

176   (Bougiatioti et al., 2014; Liu et al., 2015). MO-OOA may be related to aqueous-phase processing

177   (Xu et al., 2016; Yu et al., 2014). Recent studies hypothesize that the rapidly produced HOMs

178   (highly oxygenated molecules) from the oxidation of volatile organic compounds (VOCs) likely

179   contribute to MO-OOA (Ehn et al., 2014). In this study, MO-OOA only increases in 1 out of 19

180   α-pinene experiments, suggesting that HOMs unlikely contribute to MO-OOA. While HOMs can

181   be lost to chamber wall or sampling lines, these processes do not deplete all the HOMs formed, as

182   Zhang et al. (2015) were able to detect HOMs in chamber experiments.

S4. Description of Measurements at Multiple Sites

184   We have previously performed comprehensive year-long measurements at multiple sites

185   in the southeastern U.S., as part of Southeastern Center for Air Pollution and Epidemiology study

186   (SCAPE) and Southern Oxidant and Aerosol Study (SOAS). Detailed descriptions about these

187   field studies have been discussed in the literature (Xu et al., 2015a; Xu et al., 2015b). The sampling

188   periods are shown in Table S1 and the sampling sites are briefly discussed below.

189 • Georgia Tech site (GT, 33.78 N, 84.40 W): This site is located on the rooftop of the
190 Environmental Science and Technology (ES&T) building on the Georgia Institute of Technology
191 (GT) campus, which is about 30-40m above the ground and 840m away from interstate I75/85.
192 The ambient perturbation experiments were performed at this site.

193 • Jefferson Street site (JST, 33.78 N, 84.42 W): This is a central SEARCH (SouthEastern Aerosol
194 Research and Characterization) site, which is in Atlanta's urban area with a mixed commercial and
195 residential neighborhood. It is about 2 km west of the Georgia Tech site. The JST and GT sites are
196 in the same grid cell in CMAQ.

197 • Yorkville site (YRK, 33.93 N, 85.05 W): This is a central SEARCH site located in a rural area
198 in Georgia. This site is surrounded by agricultural land and forests and is at about 80 km northwest
199 of JST site.

200 • Centreville site (CTR, 32.94°N, 87.18°W): This is a central SEARCH site in rural Alabama. The
201 sampling site is surrounded by forests and away from large urban areas (55km SE and 84 km SW
202 of Tuscaloosa and Birmingham, AL, respectively).

203   In addition to the perturbation experiments in 2016, we deployed AMS measurements in
204 summer of 2012, 2013, and 2015 (Table S5) at the GT site (Xu et al., 2015a; Xu et al., 2017). The
205 same five OA factors are resolved and the mass fractions of these OA factors do not change
206 substantially over the past 5 years (Fig. S8), suggesting relatively stable OA sources over the past
207 5 years near this measurement site.

208   The 2012 measurements are used for the pseudo-experiment discussed in Appendix A. It
209 is because the 2012 data set has the least interruption in ambient measurements. For example, in
210 2016, the perturbation experiments resulted in many gaps in the ambient measurements. In 2013,
211 AMS alternated sampling between ambient line and a treated sampling line every 30min (Xu et
212 al., 2017). Since measurements were performed around similar time of year each year and the mass
213 fractions of these OA factors remain relatively constant over the past 5 years, this justifies the use
214 2012 data set for the pseudo-experiment (i.e., this data set can be considered as representative of
215 other years).

S5. Community Multiscale Air Quality (CMAQ) Model

We use the CMAQ (Community Multiscale Air Quality) atmospheric chemical transport model to simulate the SOA formation in the southeastern U.S. CMAQ is one of the most widely used air quality models. CMAQ v5.2gamma (available at: https://github.com/USEPA/CMAQ) is run over the continental U.S. for time periods between May 2012 to July 2013 with 12km × 12km horizontal resolution. We focus our analysis on the southeastern U.S., which comprises 11 states (as Arkansas, Alabama, Florida, Georgia, Kentucky, Louisiana, Mississippi, North Carolina, South Carolina, Tennessee, and Virginia). 10 days of model spin-up are discarded before comparisons are made with measurements. The meteorological inputs are generated with version 3.8 of the Weather Research and Forecasting model (WRF), Advanced Research WRF (ARW) core. Compared to previous versions of WRF, WRF v3.8 has major revisions in the vertical mixing scheme (Appel et al., 2017). We also apply lightning assimilation to improve convective rainfall (Heath et al., 2016). Anthropogenic emissions are based on the EPA (Environmental Protection Agency) NEI (National Emission Inventory) 2011 v2. For the CTR_June period, the primary emissions from stationary source fuel combustion and industry are reduced to half in Alabama, because previous studies showed that CMAQ overestimates the primary organic carbon in Alabama during this period (Pye et al., 2015). Biogenic emissions are predicted by the BEIS (Biogenic Emission Inventory System) v3.6.1. Carlton and Baker (2011) found that the BEIS predicted isoprene emission is generally lower than that predicted by another widely used model MEGAN (Model of Emissions of Gases and Aerosols from Nature). Also, Pye et al. (2017) showed that increasing the BEIS predicted isoprene emission by 50% could result in a better agreement with measured isoprene and OH at Centreville, AL. Thus, the isoprene emission is increased by 50% in this study.

The gas-phase chemistry is based on CB6r3 (Carbon Bond v6.3, http://www.camx.com/files/udaq_snowchem_final_6aug15.pdf). The default CMAQv5.2gamma organic aerosol treatment in CMAQ v5.2gamma generally follows the scheme of Carlton et al. (2010) and Appel et al. (2017). A schematic of SOA treatment in CMAQ v5.2gamma is shown in Fig. S1a. In brief, CMAQ v5.2gamma includes SOA formation from anthropogenic and biogenic emissions. Anthropogenic precursors include benzene, toluene, xylene, long-chain alkanes (such as heptadecane), and PAHs (such as naphthalene). Biogenic precursors include isoprene, monoterpenes, and sesquiterpenes. An Odum 2-product parameterization is used to describe SOA

247   formation from these precursors. The SOA yields from monoterpene reactions with different

248   oxidants (OH, ozone) are assumed to be the same and are based on daylight experiments of Griffin

249   et al. (1999) The SOA yield from sesquiterpenes oxidation is parameterized in an analogous way

250   as that of monoterpenes (Carlton et al., 2010). Five different species of monoterpenes are lumped

251   into one species (i.e., TERP) according to U.S. emissions-based weighting factors. SOA formation

252   from the reactive uptake of IEPOX and methacryloylperoxynitrate (MPAN) (isoprene oxidation

253   products) onto aqueous aerosol is included. All semi-volatile OA in the model can undergo

254   particle-phase oligomerization to produce non-volatile OA with a 29hr lifetime. POA is treated as

255   semi-volatile. A parameterization to consider the SOA from semivolatile and intermediate

256   volatility organic compounds (SVOC and IVOC, the emissions of which may not be characterized

257   in current emission inventories) as well as other missing sources of SOA from anthropogenic

258   combustion (potentially due to underestimated yields) is implemented (Murphy et al., 2017).

259   The "default simulation" applies the default treatment of SOA in CMAQ v5.2gamma with

260   CB6r3 as discussed above. The "updated simulation" in this work improves the "default simulation"

261   by implementing the following recent scientific findings (Fig. S1b). Firstly, recent laboratory

262   studies reveal significant amount of SOA formation from monoterpenes (except α-pinene, denoted

263   as $MT_{w/o\ \alpha\text{-pinene}}$) oxidation by NO_3 (Boyd et al., 2015; Fry et al., 2014). This SOA formation

264   pathway is currently missing in CMAQ v5.2gamma with CB6r3 chemistry. We implement the

265   formation and partition of organic nitrates from monoterpenes via multiple reaction pathways (i.e.,

266   oxidation by NO_3 and oxidation by OH/O_3 followed by RO_2+NO), which are extensively described

267   in Pye et al. (2015). In brief, the organic nitrates produced from $MT_{w/o\ \alpha\text{-pinene}}$ oxidation by NO_3

268   and MT oxidation by OH and O_3 in the presence of NO_x are lumped into a new species: $MTNO_3$.

269    $MTNO_3$ is semi-volatile and undergoes gas/particle partitioning. The particle-phase $MTNO_3$

270   hydrolyzes with a 3hr lifetime and converts to HNO_3 and non-volatile SOA (denoted as AMTHYD

271   in model). We note that the hydrolysis rate of organic nitrates is highly uncertain, which largely

272   depends on the structure of organic nitrates and particle acidity (Boyd et al., 2015; Jacobs et al.,

273   2014; Rindelaub et al., 2016). Pye et al. compared model performance using 3hr vs 30hr hydrolysis

274   rate (Pye et al., 2015). While the 3hr hydrolysis rate leads to better agreements with measured OC

275   and NO_y, it degrades the comparison with measured HNO_3. In this study, we perform sensitivity

276   study by using both 3hr and 30hr hydrolysis rate. 30hr hydrolysis lower the modeled SOA_{MT+SQT}

277   concentration by 2-17% for all sites compared to 3hr hydrolysis, but it does not change the

278   conclusion of this study. Future studies are warranted to constrain the fate of organic nitrates.

279   The second modification is to update the SOA yield of the monoterpenes oxidation by O_3

280   and OH. In the default SOA treatment, the SOA yield of lumped monoterpenes oxidation by O_3

281   and OH is parameterized based on daylight experiments of Griffin et al. (1999), which are under

282   high OA loadings and temperature. Extrapolation of the parameterized yield to atmospherically

283   relevant low OA loading and lower temperatures (<310K) causes uncertainty (Pathak et al., 2007).

284   In this study, we update the SOA yield of monoterpenes oxidation by O_3 and OH based on a recent

285   study by Saha and Grieshop (2016). Saha et al. applied a dual-thermodenuder system to study the

286   α-pinene ozonolysis SOA. The authors extracted SOA yield parameters by using an evaporation-

287   kinetics model and volatility basis set (VBS). The SOA yields in Saha et al. (2016) are higher than

288   laboratory chamber studies conducted in batch mode (Griffin et al., 1999; Pathak et al., 2007), but

289   comparable to laboratory chamber studies conducted in continuous mode (Shilling et al., 2008)

290   (Fig. S9). The SOA yields in Saha et al. are consistent with recent findings about the formation of

291   HOMs (Ehn et al., 2014; Zhang et al., 2015) and help to explain the observed slow evaporation of

292   α-pinene SOA (Vaden et al., 2011). In the updated simulation, we replace the Odum's 2-product

293   model used in the default simulation with VBS framework. The VBS framework lumps species

294   into a number of volatility "bins" that are separated by one decade in saturation concentration.

295   When laboratory data are available over a wide range of loadings and/or temperatures, the VBS

296   framework is more robust and better represents SOA formation at atmospherically relevant OA

297   loadings than Odum's 2-product model with limited data (Barsanti et al., 2013). The properties of

298   the lumped MT oxidation products, which are grouped into 7 volatility "bins", are listed in Table

299   S3. The simulation using modified SOA treatment is denoted as "updated simulation".

300   The modeled OA concentrations from both default simulation and updated simulation are

301   compared to AMS measurements. Considering that CMAQ predicts aerosol in 3 log-normal modes

302   and AMS measures PM_1, the modeled mass concentration is adjusted to PM_1 based on predicted

303   aerosol size distributions (Nolte et al., 2015). CMAQ predicts that PM_1 concentration accounts for

304   about 60-70% of $PM_{2.5}$ concentration. This fraction is similar to the finding in Zhang et al. (2017),

305   who performed simultaneous measurements of non-refractory $PM_{2.5}$ (using an AMS with a new

306    $PM_{2.5}$ inlet) and non-refractory PM_1 (using an AMS with a traditional PM_1 inlet) in Nanjing, China.

307   The authors showed that non-refractory PM_1 accounts for about half of non-refractory $PM_{2.5}$. The

308 PM$_1$/PM$_{2.5}$ fraction needs to be further verified for sites in the U.S. Fig. S10 compares the diurnal

309 trends of AMS OA with CMAQ OA in both default simulation and updated simulation. The JST

310 and GT sites are in the same grid cell in CMAQ. The modeled OA in default simulation under-

311 estimates measured OA by 36-54%. The updated simulation predicts more OA, which reduces

312 model bias and agrees better with measured OA. The model skill in updated simulation is slightly

313 improved as the correlation between model and measurement is better (Fig. S11). However, the

314 updated simulation still under-estimates OA, mainly in the afternoon, suggesting missing OA

315 sources.

316 We further evaluate the modeled SOA from the oxidation of monoterpenes and

317 sesquiterpenes (SOA$_{MT+SQT}$) against LO-OOA. Based on the ambient perturbation experiments,

318 84% of fresh α-pinene SOA is apportioned into LO-OOA and the rest 16% is apportioned into

319 isoprene-OA (Fig. S7a), when the isoprene-OA factor exists. Thus, for the sites with isoprene-OA

320 factor, we only consider 84% of modeled SOA from the oxidation of monoterpenes by O$_3$ and OH

321 when comparing to LO-OOA. We note that the fraction of MT SOA apportioned into isoprene-

322 OA factor is uncertain, as this value is obtained at a specific site and in a specific month. This

323 uncertainty may affect the comparison between modeled SOA$_{MT+SQT}$ and LO-OOA. More studies

324 are required to evaluate the interference of MT SOA in isoprene-OA factor in different atmospheric

325 environments and different seasons. The comparison between LO-OOA and SOA$_{MT+SQT}$ is

326 discussed in the main text and shown in Fig. 8, Fig. S12, and Fig. S13. We note that the modeled

327 SOA$_{MT+SQT}$ in updated simulation agrees within 20% of LO-OOA for all sites, except CTR_June.

328 For CTR_June, the modeled SOA$_{MT+SQT}$ is higher than LO-OOA by ~43%. The reason for the

329 over-estimation of LO-OOA in CTR_June is unclear. One possible reason is that CMAQ over-

330 predicts the role of primary organic emissions and subsequent OA formation from these emissions,

331 which serve as gas/particle partition medium. This suggests that the parameterized potential SOA

332 from combustion sources (i.e., pcSOA) may need downward adjustment (Murphy et al., 2017).

333 The sampling site in CTR is surrounded by forests and is far away from stationary point and area

334 sources of primary emissions. The marginal influence of primary emissions on the CTR site can

335 be reflected by that HOA factor is not resolved from PMF analysis. However, the grid cell

336 containing the CTR site has primary emissions. Pye et al. (2015) showed that the POA

337 concentration is over-estimated by a factor of 2 in CTR_June when POA is treated as non-volatile.

338 As gas/particle partition medium, a higher POA concentration would enhance the partition of semi-

339   volatiles to the particle phase and hence increase the concentration of modeled SOA. The

340   implementation of SOA formation from SVOC and IVOC, mainly from anthropogenic emissions,

341   further exaggerates the issue. Another possible reason is that the parameterization of MT SOA

342   formation does not consider photo-chemical aging. The laboratory experiments used to derive

343   SOA yield parameters typically only last few hours. The aging of SOA is likely to decrease the

344   concentration after long time periods due to fragmentation. In addition, previous work by Pye et

345   al. (2015), albeit with different meteorology indicates monoterpenes as well as their organic

346   nitrates are overestimated by CMAQ in the vicinity of CTR. Errors in nocturnal mixing may

347   contribute to errors in SOA, particularly from monoterpenes.

348   **S6. Simple Box Model**

349   While the focus of this study is to qualitatively understand which OA factors the α-pinene

350   SOA is apportioned into, we also build a simple box model aimed at quantitively estimate the fate

351   of α-pinene and the SOA formation in the ambient perturbation experiments. The box model

352   considers the oxidation of α-pinene by OH and O$_3$, dilution by ambient air, and particle loss to

353   chamber wall. We solve the following two ordinary differential equations (ODEs) which are

354   derived from mass balance.

355

$$\frac{d[\alpha\text{-pinene}]}{dt} = -k_{OH} \times [\alpha\text{-pinene}] \times [OH] - k_{O_3} \times [\alpha\text{-pinene}] - \frac{F_{out}}{V_{chamber}} \times [\alpha\text{-pinene}] \qquad \text{Eq. S1}$$

$$\frac{d[SOA]}{dt} = Yield \times (k_{OH} \times [\alpha\text{-pinene}] \times [OH] + k_{O_3} \times [\alpha\text{-pinene}] \times [O_3]) \times 5.6 - \frac{F_{out}}{V_{chamber}} \times [SOA] \qquad \text{Eq. S2}$$

356   F_{out} is the dilution rate, which is 20 LPM (estimated by sampling flow rates of all instruments).

357    $V_{chamber}$ is the chamber volume, which is about 2 m^3. k_{OH} and k_{O3} are the reaction rate constants

358   for α-pinene + OH and α-pinene + O$_3$,which are 5.25×10^{-11} and 9.40×10^{-17} cm^3 molecule^{-1} s^{-1} at

359   298K, respectively (Jenkin et al., 1997). The constant 5.6 is to convert the α-pinene concentration

360   unit from ppb to μg m^{-3}. *Yield* is defined as the ratio of the amount of SOA formed to the amount

361   of VOC reacted (Odum et al., 1996), which is assumed to the same for the oxidation of α-pinene

362   by OH and O$_3$. The ambient perturbation approach is potentially feasible to directly measure the

363   SOA yield under real atmospheric conditions. However, certain improvements are required, such

364   as measuring the concentration of precursor VOC and quantifying the dilution ratio. In the current

365   box model, *yield* is a tuning parameter. The model only considers the SOA formed from α-pinene

366 injected into the chamber and neglects the inflow ambient OA and α-pinene. Thus, the model

367 results can be directly compared to the LO-OOA enhancement amount.

368   We use the simple box model to simulate experiment ap_0801_1. The O_3 concentration

369 measured during this experiment is ~55 ppb. The OH concentration is not measured, but assumed

370 to be 1×10^6 or 2×10^6 molecule cm^{-3} as sensitivity tests. The particle wall loss is difficult to

371 characterize because the eight corners of the bag are open, so that the change in particle number

372 concentration can be due to both wall loss and ambient variation. Moreover, the particle wall loss

373 may vary between experiments because the wind affects the movement of chamber walls and hence

374 the particle wall loss. Thus, we assume the particle wall loss rate to be 1×10^{-4} s^{-1}, which is 100

375 times higher than the loss rate of 200nm particles in the Georgia Tech Environmental Chamber

376 facility (Nah et al., 2016) and serves as an upper bound of loss rate. We find that the wall loss rate

377 has negligible effects on particle mass concentration, compared to other factors.

378   Fig. S14 shows the results from the simple box model. Although ~14 ppb α-pinene is

379 injected, most of α-pinene is carried out of the chamber due to dilution with ambient air (Fig. S14a).

380 Only 2-5 ppb α-pinene reacts with oxidants (i.e., O_3 and OH) after 40 min. For the reacted α-pinene,

381 roughly half reacts with O_3 and the other half reacts with OH. Fig. S14a also shows the simulated

382 time series of SOA by using a range of yields. The box model can predict the measured

383 enhancement amount in SOA using SOA yields of 20-30%, which is consistent with yields

384 measured from laboratory studies (Saha and Grieshop, 2016; Shilling et al., 2008). Despite the

385 agreement in magnitude, the predicted SOA concentration peaks later and decreases slower than

386 measurements. Possible reasons include non-ideal mixing and/or existence of a dead zone in the

387 chamber. Assuming a 1.75 m^3 dead zone in the 2 m^3 chamber can reasonably simulate the temporal

388 profile of measured SOA (Fig. S14b). However, a SOA yield of ~100% is required to match the

389 enhancement magnitude, which is roughly 10 times higher than reported yields from laboratory

390 studies and likely unreasonable. Another uncertain parameter in the box model is the dilution rate.

391 Increasing the dilution rate would have the same effect as increasing the volume of dead zone. The

392 dilution rate is estimated to be 20 LPM as determined by the pulling rates of all instruments. This

393 dilution rate is better constrained than the volume of dead zone since the instrument sampling rates

394 are known. The reasons for the discrepancy in OA decrease rate between model and measurements

395 are unclear, but likely due to a combination of dead zone volume and dilution rate. To understand

396 this discrepancy, future studies with adequate measurements of more species, particularly the

14

397   VOCs, are required. The improved experiments could provide better estimate of SOA yields under

398   real ambient conditions. Palm et al. (2017) attempted to quantify the SOA yields from the

399   individual VOC by oxidizing VOC in an oxidation flow reactor (OFR) with ambient air. Note that

400   the extra oxidation is added in the OFR in Palm et al. (2017), which is different from this study.

401   The discrepancy between model and measurements in either the magnitude or the decrease rate

402   does not influence the conclusions in this study, as our focus is to qualitatively understand which

403   OA factors the α-pinene SOA is apportioned into.

404   The OA formation in perturbation experiments with isoprene or *m*-xylene is below the

405   detection limit of the experimental approach. This is mainly due to the low SOA yields or slow

406   oxidation rates of these VOCs (Ng et al., 2007). We used the simple box model to simulate the

407   perturbation experiments with isoprene and *m*-xylene. For *m*-xylene experiments, about 90 ppb is

408   injected. However, due to the slow oxidation rate of *m*-xylene, small SOA yield (i.e., ~5% in Ng

409   et al. (2007)), and large dilution by ambient air, it is estimated that only about 4 ppb *m*-xylene

410   reacts with OH after 40min and produces ~0.15-0.30 $\mu g\ m^{-3}$ SOA (Fig. S14c). For isoprene,

411   although its oxidation rate is fast, its SOA yield from non-IEPOX route is low (Xu et al., 2014;

412   Kroll et al., 2006). The isoprene oxidation products which form SOA are mostly second or higher

413   generation products. They are not formed in large amount in the relatively short perturbation

414   experiments (i.e., 40min).

415   **S7. Laboratory Study on SOA Formation from α-pinene**

416   We performed laboratory experiments to study the SOA formation from α-pinene under

417   different NO_x conditions in the Georgia Tech Environmental Chamber (GTEC) facility. The

418   facility consists of two 12 m^3 Teflon chambers, which are suspended inside a temperature-

419   controlled enclosure and surrounded by black lights. The detailed description about chamber

420   facility can be found in Boyd et al. (2015) The experimental procedures have been discussed in

421   Tuet et al. (2017) In brief, the chambers are flushed with clean air prior to each experiment. Then,

422   α-pinene and oxidant sources (i.e., H_2O_2, NO_2, or HONO) are injected into chamber. Once the

423   concentrations of species stabilize, the black lights are turned on to initiate photooxidation. The

424   SOA generated by using H_2O_2 (i.e., NO-free condition), NO_2 (i.e., mid-NO condition), and HONO

425   (i.e., high NO condition) as oxidant sources are denoted as $SOA_{lab,H2O2}$, $SOA_{lab,NO2}$, and

426   $SOA_{lab,HONO}$, respectively.

427   The experimental conditions are summarized in Table S2. We note that more than 100ppb
428   α-pinene is injected in the experiments using H_2O_2 and HONO. It is because these two experiments
429   were designed to produce large amounts of SOA for filter collection and offline analysis (Tuet et
430   al., 2017). Considering that the OA concentration affects the partitioning of semi-volatile organic
431   compounds and hence affects the organic mass spectra measured by AMS, we calculate the
432   average mass spectra in these laboratory studies by only using the data when the OA concentration
433   is below 10 $\mu g\ m^{-3}$, which is similar to that in our ambient perturbation experiments.

434   The mass spectra of each laboratory-generated SOA (denoted as SOA_{lab}) are compared
435   against the mass spectra of α-pinene SOA generated during perturbation experiments (denoted as
436   "$SOA_{ambient}$"). The correlation coefficients (R) between the mass spectra of SOA_{lab} and $SOA_{ambient}$
437   are plotted against the NO concentration during ambient perturbation experiments. We calculate
438   the organic mass spectra of $SOA_{ambient}$ in the following way. Firstly, we scale the magnitude of the
439   OA mass spectrum during Chamber_Bf period by the ratio of OA concentration during the
440   Chamber_Bf period to that during the extrapolated Chamber_Bf period. Secondly, we subtract this
441   scaled OA mass spectrum from that during the Chamber_Af period. Thirdly, we normalize the
442   "difference mass spectra" to the difference in organic signal. It is important to note that this
443   calculation is only performed for the experiments with significant formation of total OA. The
444   comparison results are discussed in the main text.

445   When comparing the mass spectra of $SOA_{ambient}$ with SOA_{lab}, we note that the mass
446   spectrua of $SOA_{ambient}$ (when ambient NO is > 0.3ppb) generally agree better with that of
447    $SOA_{lab,NO2}$ than $SOA_{lab,HONO}$. This suggest that the laboratory experiment using NO_2+hv as oxidant
448   source is more representative of ambient high NO conditions than HONO+hv. This is likely due
449   to the following reasons. Firstly, from the simple box model, we estimate that about half of α-
450   pinene reacts with OH and the other half reacts with O_3 in the perturbation experiments, which is
451   similar to that in laboratory experiments with NO_2+hv (Table S2). In contrast, the fate of α-pinene
452   is dominated by OH in HONO+hv experiment. Secondly, the NO_x level and NO/NO_2 ratio in
453   perturbation experiments are more similar to those in the NO_2+hv experiment than the HONO
454   experiment. For example, the NO/NO_2 ratio in α-pinene perturbation experiments ranges between
455   0.03 and 0.4, which is closer to the range in NO_2+hv experiment (0.1-0.4) than in HONO
456   experiment (0.4-0.9). Thirdly, while both perturbation experiments and NO_2+hv experiment have

457 high RH (>40%), the RH in HONO+hν experiment is <5%. However, we expect the effects of
458 different RH on the mass spectra comparison are much smaller compared to the first two reasons.

S8. Estimate the Fate of RO₂ in the Atmosphere

459 **S8. Estimate the Fate of RO_2 in the Atmosphere**

460 The plateaus in Fig. 6 indicate that when NO is ~0.3ppb, RO_2+NO is the dominant fate of
461 RO_2. This NO level (~0.3ppb) is consistent with the NO level required to dominate the fate of RO_2,
462 as calculated by using previously measured HO_2 and kinetic rate constants.

463 According to Master Chemical Mechanism (MCM v3.3) (Jenkin et al., 1997; Saunders et
464 al., 2003), the reaction rates of RO_2+NO and RO_2+HO_2 are listed below.

465
$$k_{RO_2+NO} = 2.7e\text{-}12 \times \exp(360/T) = 9.04e\text{-}12 \text{ cm}^3 \text{ molecule}^{-1} \text{ s}^{-1} \text{ (@298K)}$$
$$k_{RO_2+HO_2} = 2.91e\text{-}13 \times \exp(1300/T) = 2.28e\text{-}11 \text{ cm}^3 \text{ molecule}^{-1} \text{ s}^{-1} \text{ (@298K)}$$

466 The afternoon HO_2 concentration is about 5-20ppt from previous measurements at the same site
467 during a similar period (Sanchez et al., 2016; Chen et al., 2017). Thus, when the NO concentration
468 is about 0.1-0.5 ppb, RO_2+NO would be 10 times faster than RO_2+HO_2 and NO dominates the fate
469 of RO_2. This is similar to the estimated 0.2-0.3 ppb based on the comparison in organic mass
470 spectra between SOA_ambient and SOA_lab.

471 **S9. More discussions on β-caryophyllene perturbation experiments.**

472 The concentrations of MO-OOA and isoprene-OA decrease after injecting β-caryophyllene.
473 The reason for the decrease in MO-OOA and isoprene-OA is unclear, but likely due to the
474 limitations of PMF analysis, that is, PMF assumes constant mass spectra of OA factors. After β-
475 caryophyllene SOA formation in the chamber, in order to optimize the overall fitting residual,
476 PMF solver increases the concentrations of LO-OOA and COA, the mass spectra of which are
477 more similar to β-caryophyllene SOA, and decreases the concentration of MO-OOA and isoprene-
478 OA, which have relatively different mass spectra as β-caryophyllene SOA. This likely causes the
479 reduction in MO-OOA and isoprene-OA concentrations. Similar issue has been observed in
480 previous studies.

481 One interesting finding in β-caryophyllene perturbation experiments is that the LO-OOA
482 enhancement amount is greatly affected by NO_2 level. More LO-OOA is formed in perturbation
483 experiments with a lower NO_2 level (Fig. S15f), when the O_3 concentration and injection time are

484   similar. The reason for this NO_2 effect on β-caryophyllene SOA is currently unknown. Considering

485   that the major fate of β-caryophyllene in the ambient perturbation experiments is reaction with O_3

486   (i.e., lifetimes of β-caryophyllene with respect to 40ppb O_3 and 10^6 molecules cm^{-3} OH are 1.5min

487   and 80min, respectively), the NO_2 effect may be related to Criegee radical, which is the most

488   important intermediate radical in ozonolysis of alkenes. In terms of the roles of NO_x in SOA

489   formation from β-caryophyllene, previous laboratory studies have mostly focused on the β-

490   caryophyllene oxidation by OH (Tasoglou and Pandis, 2015) instead of oxidation by O_3 (i.e., the

491   atmospherically dominant fate of β-caryophyllene). Thus, the effects of NO_2 on SOA formation

492   from the ozonolysis of β-caryophyllene warrants future studies.

Reference

Appel, K. W., Napelenok, S. L., Foley, K. M., Pye, H. O. T., Hogrefe, C., Luecken, D. J., Bash, J. O., Roselle, S. J., Pleim, J. E., Foroutan, H., Hutzell, W. T., Pouliot, G. A., Sarwar, G., Fahey, K. M., Gantt, B., Gilliam, R. C., Heath, N. K., Kang, D., Mathur, R., Schwede, D. B., Spero, T. L., Wong, D. C., and Young, J. O.: Description and evaluation of the Community Multiscale Air Quality (CMAQ) modeling system version 5.1, Geosci. Model Dev., 10, 1703-1732, 10.5194/gmd-10-1703-2017, 2017.

Barsanti, K. C., Carlton, A. G., and Chung, S. H.: Analyzing experimental data and model parameters: implications for predictions of SOA using chemical transport models, Atmos. Chem. Phys., 13, 12073-12088, 10.5194/acp-13-12073-2013, 2013.

Bougiatioti, A., Stavroulas, I., Kostenidou, E., Zarmpas, P., Theodosi, C., Kouvarakis, G., Canonaco, F., Prévôt, A. S. H., Nenes, A., Pandis, S. N., and Mihalopoulos, N.: Processing of biomass-burning aerosol in the eastern Mediterranean during summertime, Atmos. Chem. Phys., 14, 4793-4807, 10.5194/acp-14-4793-2014, 2014.

Boyd, C. M., Sanchez, J., Xu, L., Eugene, A. J., Nah, T., Tuet, W. Y., Guzman, M. I., and Ng, N. L.: Secondary organic aerosol formation from the β-pinene+NO3 system: effect of humidity and peroxy radical fate, Atmos. Chem. Phys., 15, 7497-7522, 10.5194/acp-15-7497-2015, 2015.

Budisulistiorini, S. H., Canagaratna, M. R., Croteau, P. L., Marth, W. J., Baumann, K., Edgerton, E. S., Shaw, S. L., Knipping, E. M., Worsnop, D. R., Jayne, J. T., Gold, A., and Surratt, J. D.: Real-Time Continuous Characterization of Secondary Organic Aerosol Derived from Isoprene Epoxydiols in Downtown Atlanta, Georgia, Using the Aerodyne Aerosol Chemical Speciation Monitor, Environ Sci Technol, 47, 5686-5694, Doi 10.1021/Es400023n, 2013.

Budisulistiorini, S. H., Li, X., Bairai, S. T., Renfro, J., Liu, Y., Liu, Y. J., McKinney, K. A., Martin, S. T., McNeill, V. F., Pye, H. O. T., Nenes, A., Neff, M. E., Stone, E. A., Mueller, S., Knote, C., Shaw, S. L., Zhang, Z., Gold, A., and Surratt, J. D.: Examining the effects of anthropogenic emissions on isoprene-derived secondary organic aerosol formation during the 2013 Southern Oxidant and Aerosol Study (SOAS) at the Look Rock, Tennessee ground site, Atmos. Chem. Phys., 15, 8871-8888, 10.5194/acp-15-8871-2015, 2015.

Canagaratna, M. R., Jayne, J. T., Jimenez, J. L., Allan, J. D., Alfarra, M. R., Zhang, Q., Onasch, T. B., Drewnick, F., Coe, H., Middlebrook, A., Delia, A., Williams, L. R., Trimborn, A. M., Northway, M. J., DeCarlo, P. F., Kolb, C. E., Davidovits, P., and Worsnop, D. R.: Chemical and microphysical characterization of ambient aerosols with the aerodyne aerosol mass spectrometer, Mass Spectrometry Reviews, 26, 185-222, 10.1002/mas.20115, 2007.

534 Canagaratna, M. R., Jimenez, J. L., Kroll, J. H., Chen, Q., Kessler, S. H., Massoli, P., Hildebrandt
535 Ruiz, L., Fortner, E., Williams, L. R., Wilson, K. R., Surratt, J. D., Donahue, N. M., Jayne, J. T.,
536 and Worsnop, D. R.: Elemental ratio measurements of organic compounds using aerosol mass
537 spectrometry: characterization, improved calibration, and implications, Atmos. Chem. Phys., 15,
538 253-272, 10.5194/acp-15-253-2015, 2015.
539

540 Carlton, A. G., Bhave, P. V., Napelenok, S. L., Edney, E. O., Sarwar, G., Pinder, R. W., Pouliot,
541 G. A., and Houyoux, M.: Model Representation of Secondary Organic Aerosol in CMAQv4.7,
542 Environ Sci Technol, 44, 8553-8560, 10.1021/es100636q, 2010.
543

544 Carlton, A. G., and Baker, K. R.: Photochemical Modeling of the Ozark Isoprene Volcano:
545 MEGAN, BEIS, and Their Impacts on Air Quality Predictions, Environ Sci Technol, 45, 4438-
546 4445, 10.1021/es200050x, 2011.
547

548 Cerully, K. M., Bougiatioti, A., Hite Jr, J. R., Guo, H., Xu, L., Ng, N. L., Weber, R., and Nenes,
549 A.: On the link between hygroscopicity, volatility, and oxidation state of ambient and water-
550 soluble aerosols in the southeastern United States, Atmos. Chem. Phys., 15, 8679-8694,
551 10.5194/acp-15-8679-2015, 2015.
552

553 Chan, M. N., Chan, A. W. H., Chhabra, P. S., Surratt, J. D., and Seinfeld, J. H.: Modeling of
554 secondary organic aerosol yields from laboratory chamber data, Atmos. Chem. Phys., 9, 5669-
555 5680, 10.5194/acp-9-5669-2009, 2009.
556

557 Chen, D., Huey, L. G., Tanner, D. J., Li, J., Ng, N. L., and Wang, Y.: Derivation of Hydroperoxyl
558 Radical Levels at an Urban Site via Measurement of Pernitric Acid by Iodide Chemical Ionization
559 Mass Spectrometry, Environ Sci Technol, 10.1021/acs.est.6b05169, 2017.
560

561 Chen, Q., Farmer, D. K., Rizzo, L. V., Pauliquevis, T., Kuwata, M., Karl, T. G., Guenther, A.,
562 Allan, J. D., Coe, H., Andreae, M. O., Pöschl, U., Jimenez, J. L., Artaxo, P., and Martin, S. T.:
563 Submicron particle mass concentrations and sources in the Amazonian wet season (AMAZE-08),
564 Atmos. Chem. Phys., 15, 3687-3701, 10.5194/acp-15-3687-2015, 2015.
565

566 Crippa, M., Canonaco, F., Lanz, V. A., Äijälä, M., Allan, J. D., Carbone, S., Capes, G., Ceburnis,
567 D., Dall'Osto, M., Day, D. A., DeCarlo, P. F., Ehn, M., Eriksson, A., Freney, E., Hildebrandt Ruiz,
568 L., Hillamo, R., Jimenez, J. L., Junninen, H., Kiendler-Scharr, A., Kortelainen, A. M., Kulmala,
569 M., Laaksonen, A., Mensah, A. A., Mohr, C., Nemitz, E., O'Dowd, C., Ovadnevaite, J., Pandis, S.
570 N., Petäjä, T., Poulain, L., Saarikoski, S., Sellegri, K., Swietlicki, E., Tiitta, P., Worsnop, D. R.,
571 Baltensperger, U., and Prévôt, A. S. H.: Organic aerosol components derived from 25 AMS data
572 sets across Europe using a consistent ME-2 based source apportionment approach, Atmos. Chem.
573 Phys., 14, 6159-6176, 10.5194/acp-14-6159-2014, 2014.
574

575 de Sá, S. S., Palm, B. B., Campuzano-Jost, P., Day, D. A., Newburn, M. K., Hu, W., Isaacman-
576 VanWertz, G., Yee, L. D., Thalman, R., Brito, J., Carbone, S., Artaxo, P., Goldstein, A. H., Manzi,

577 A. O., Souza, R. A. F., Mei, F., Shilling, J. E., Springston, S. R., Wang, J., Surratt, J. D., Alexander,
578 M. L., Jimenez, J. L., and Martin, S. T.: Influence of urban pollution on the production of organic
579 particulate matter from isoprene epoxydiols in central Amazonia, Atmos. Chem. Phys. Discuss.,
580 2016, 1-58, 10.5194/acp-2016-1020, 2016.
581

582 de Sá, S. S., Palm, B. B., Campuzano-Jost, P., Day, D. A., Newburn, M. K., Hu, W., Isaacman-
583 VanWertz, G., Yee, L. D., Thalman, R., Brito, J., Carbone, S., Artaxo, P., Goldstein, A. H., Manzi,
584 A. O., Souza, R. A. F., Mei, F., Shilling, J. E., Springston, S. R., Wang, J., Surratt, J. D., Alexander,
585 M. L., Jimenez, J. L., and Martin, S. T.: Influence of urban pollution on the production of organic
586 particulate matter from isoprene epoxydiols in central Amazonia, Atmos. Chem. Phys., 17, 6611-
587 6629, 10.5194/acp-17-6611-2017, 2017.
588

589 DeCarlo, P. F., Kimmel, J. R., Trimborn, A., Northway, M. J., Jayne, J. T., Aiken, A. C., Gonin,
590 M., Fuhrer, K., Horvath, T., Docherty, K. S., Worsnop, D. R., and Jimenez, J. L.: Field-Deployable,
591 High-Resolution, Time-of-Flight Aerosol Mass Spectrometer, Anal Chem, 78, 8281-8289,
592 10.1021/ac061249n, 2006.
593

594 Donahue, N. M., Epstein, S. A., Pandis, S. N., and Robinson, A. L.: A two-dimensional volatility
595 basis set: 1. organic-aerosol mixing thermodynamics, Atmos. Chem. Phys., 11, 3303-3318,
596 10.5194/acp-11-3303-2011, 2011.
597

598 Ehn, M., Thornton, J. A., Kleist, E., Sipila, M., Junninen, H., Pullinen, I., Springer, M., Rubach,
599 F., Tillmann, R., Lee, B., Lopez-Hilfiker, F., Andres, S., Acir, I.-H., Rissanen, M., Jokinen, T.,
600 Schobesberger, S., Kangasluoma, J., Kontkanen, J., Nieminen, T., Kurten, T., Nielsen, L. B.,
601 Jorgensen, S., Kjaergaard, H. G., Canagaratna, M., Maso, M. D., Berndt, T., Petaja, T., Wahner,
602 A., Kerminen, V.-M., Kulmala, M., Worsnop, D. R., Wildt, J., and Mentel, T. F.: A large source
603 of low-volatility secondary organic aerosol, Nature, 506, 476-479, 10.1038/nature13032, 2014.
604

605 Fry, J. L., Draper, D. C., Barsanti, K. C., Smith, J. N., Ortega, J., Winkler, P. M., Lawler, M. J.,
606 Brown, S. S., Edwards, P. M., Cohen, R. C., and Lee, L.: Secondary Organic Aerosol Formation
607 and Organic Nitrate Yield from NO3 Oxidation of Biogenic Hydrocarbons, Environ Sci Technol,
608 48, 11944-11953, 10.1021/es502204x, 2014.
609

610 Griffin, R. J., Cocker, D. R., Flagan, R. C., and Seinfeld, J. H.: Organic aerosol formation from
611 the oxidation of biogenic hydrocarbons, J Geophys Res-Atmos, 104, 3555-3567, Doi
612 10.1029/1998jd100049, 1999.
613

614 Heath, N. K., Pleim, J. E., Gilliam, R. C., and Kang, D.: A simple lightning assimilation technique
615 for improving retrospective WRF simulations, Journal of Advances in Modeling Earth Systems, 8,
616 1806-1824, 10.1002/2016MS000735, 2016.
617

618 Hodzic, A., Aumont, B., Knote, C., Lee-Taylor, J., Madronich, S., and Tyndall, G.: Volatility
619 dependence of Henry's law constants of condensable organics: Application to estimate

depositional loss of secondary organic aerosols, Geophysical Research Letters, 41, 4795-4804, 10.1002/2014GL060649, 2014.

Hu, W. W., Campuzano-Jost, P., Palm, B. B., Day, D. A., Ortega, A. M., Hayes, P. L., Krechmer, J. E., Chen, Q., Kuwata, M., Liu, Y. J., de Sá, S. S., McKinney, K., Martin, S. T., Hu, M., Budisulistiorini, S. H., Riva, M., Surratt, J. D., St. Clair, J. M., Isaacman-Van Wertz, G., Yee, L. D., Goldstein, A. H., Carbone, S., Brito, J., Artaxo, P., de Gouw, J. A., Koss, A., Wisthaler, A., Mikoviny, T., Karl, T., Kaser, L., Jud, W., Hansel, A., Docherty, K. S., Alexander, M. L., Robinson, N. H., Coe, H., Allan, J. D., Canagaratna, M. R., Paulot, F., and Jimenez, J. L.: Characterization of a real-time tracer for isoprene epoxydiols-derived secondary organic aerosol (IEPOX-SOA) from aerosol mass spectrometer measurements, Atmos. Chem. Phys., 15, 11807-11833, 10.5194/acp-15-11807-2015, 2015.

Huang, X. F., He, L. Y., Hu, M., Canagaratna, M. R., Sun, Y., Zhang, Q., Zhu, T., Xue, L., Zeng, L. W., Liu, X. G., Zhang, Y. H., Jayne, J. T., Ng, N. L., and Worsnop, D. R.: Highly time-resolved chemical characterization of atmospheric submicron particles during 2008 Beijing Olympic Games using an Aerodyne High-Resolution Aerosol Mass Spectrometer, Atmos Chem Phys, 10, 8933-8945, DOI 10.5194/acp-10-8933-2010, 2010.

Jacobs, M. I., Burke, W. J., and Elrod, M. J.: Kinetics of the reactions of isoprene-derived hydroxynitrates: gas phase epoxide formation and solution phase hydrolysis, Atmos. Chem. Phys., 14, 8933-8946, 10.5194/acp-14-8933-2014, 2014.

Jenkin, M. E., Saunders, S. M., and Pilling, M. J.: The tropospheric degradation of volatile organic compounds: a protocol for mechanism development, Atmospheric Environment, 31, 81-104, http://dx.doi.org/10.1016/S1352-2310(96)00105-7, 1997.

Jimenez, J. L., Canagaratna, M. R., Donahue, N. M., Prevot, A. S. H., Zhang, Q., Kroll, J. H., DeCarlo, P. F., Allan, J. D., Coe, H., Ng, N. L., Aiken, A. C., Docherty, K. S., Ulbrich, I. M., Grieshop, A. P., Robinson, A. L., Duplissy, J., Smith, J. D., Wilson, K. R., Lanz, V. A., Hueglin, C., Sun, Y. L., Tian, J., Laaksonen, A., Raatikainen, T., Rautiainen, J., Vaattovaara, P., Ehn, M., Kulmala, M., Tomlinson, J. M., Collins, D. R., Cubison, M. J., Dunlea, E. J., Huffman, J. A., Onasch, T. B., Alfarra, M. R., Williams, P. I., Bower, K., Kondo, Y., Schneider, J., Drewnick, F., Borrmann, S., Weimer, S., Demerjian, K., Salcedo, D., Cottrell, L., Griffin, R., Takami, A., Miyoshi, T., Hatakeyama, S., Shimono, A., Sun, J. Y., Zhang, Y. M., Dzepina, K., Kimmel, J. R., Sueper, D., Jayne, J. T., Herndon, S. C., Trimborn, A. M., Williams, L. R., Wood, E. C., Middlebrook, A. M., Kolb, C. E., Baltensperger, U., and Worsnop, D. R.: Evolution of Organic Aerosols in the Atmosphere, Science, 326, 1525-1529, DOI 10.1126/science.1180353, 2009.

Keywood, M. D., Varutbangkul, V., Bahreini, R., Flagan, R. C., and Seinfeld, J. H.: Secondary organic aerosol formation from the ozonolysis of cycloalkenes and related compounds, Environ Sci Technol, 38, 4157-4164, Doi 10.1021/Es.035363o, 2004.

Kroll, J. H., Ng, N. L., Murphy, S. M., Flagan, R. C., and Seinfeld, J. H.: Secondary organic aerosol formation from isoprene photooxidation, Environ Sci Technol, 40, 1869-1877, Doi 10.1021/Es0524301, 2006.

Lin, Y. H., Zhang, Z. F., Docherty, K. S., Zhang, H. F., Budisulistiorini, S. H., Rubitschun, C. L., Shaw, S. L., Knipping, E. M., Edgerton, E. S., Kleindienst, T. E., Gold, A., and Surratt, J. D.: Isoprene Epoxydiols as Precursors to Secondary Organic Aerosol Formation: Acid-Catalyzed Reactive Uptake Studies with Authentic Compounds, Environ Sci Technol, 46, 250-258, Doi 10.1021/Es202554c, 2012.

Liu, S., Aiken, A. C., Gorkowski, K., Dubey, M. K., Cappa, C. D., Williams, L. R., Herndon, S. C., Massoli, P., Fortner, E. C., Chhabra, P. S., Brooks, W. A., Onasch, T. B., Jayne, J. T., Worsnop, D. R., China, S., Sharma, N., Mazzoleni, C., Xu, L., Ng, N. L., Liu, D., Allan, J. D., Lee, J. D., Fleming, Z. L., Mohr, C., Zotter, P., Szidat, S., and Prevot, A. S. H.: Enhanced light absorption by mixed source black and brown carbon particles in UK winter, Nat Commun, 6, 10.1038/ncomms9435, 2015.

Matthew, B. M., Middlebrook, A. M., and Onasch, T. B.: Collection efficiencies in an Aerodyne Aerosol Mass Spectrometer as a function of particle phase for laboratory generated aerosols, Aerosol Sci Tech, 42, 884-898, Doi 10.1080/02786820802356797, 2008.

Middlebrook, A. M., Bahreini, R., Jimenez, J. L., and Canagaratna, M. R.: Evaluation of Composition-Dependent Collection Efficiencies for the Aerodyne Aerosol Mass Spectrometer using Field Data, Aerosol Sci Tech, 46, 258-271, Doi 10.1080/02786826.2011.620041, 2012.

Mohr, C., Huffman, J. A., Cubison, M. J., Aiken, A. C., Docherty, K. S., Kimmel, J. R., Ulbrich, I. M., Hannigan, M., and Jimenez, J. L.: Characterization of Primary Organic Aerosol Emissions from Meat Cooking, Trash Burning, and Motor Vehicles with High-Resolution Aerosol Mass Spectrometry and Comparison with Ambient and Chamber Observations, Environ Sci Technol, 43, 2443-2449, 10.1021/es8011518, 2009.

Murphy, B. N., Woody, M. C., Jimenez, J. L., Carlton, A. M. G., Hayes, P. L., Liu, S., Ng, N. L., Russell, L. M., Setyan, A., Xu, L., Young, J., Zaveri, R. A., Zhang, Q., and Pye, H. O. T.: Semivolatile POA and parameterized total combustion SOA in CMAQv5.2: impacts on source strength and partitioning, Atmos. Chem. Phys. Discuss., 2017, 1-44, 10.5194/acp-2017-193, 2017.

Nah, T., McVay, R. C., Zhang, X., Boyd, C. M., Seinfeld, J. H., and Ng, N. L.: Influence of seed aerosol surface area and oxidation rate on vapor wall deposition and SOA mass yields: a case study with α-pinene ozonolysis, Atmos. Chem. Phys., 16, 9361-9379, 10.5194/acp-16-9361-2016, 2016.

Ng, N. L., Kroll, J. H., Chan, A. W. H., Chhabra, P. S., Flagan, R. C., and Seinfeld, J. H.: Secondary organic aerosol formation from m-xylene, toluene, and benzene, Atmos. Chem. Phys., 7, 3909-3922, 10.5194/acp-7-3909-2007, 2007.

706

707 Ng, N. L., Canagaratna, M. R., Zhang, Q., Jimenez, J. L., Tian, J., Ulbrich, I. M., Kroll, J. H.,
708 Docherty, K. S., Chhabra, P. S., Bahreini, R., Murphy, S. M., Seinfeld, J. H., Hildebrandt, L.,
709 Donahue, N. M., DeCarlo, P. F., Lanz, V. A., Prevot, A. S. H., Dinar, E., Rudich, Y., and Worsnop,
710 D. R.: Organic aerosol components observed in Northern Hemispheric datasets from Aerosol Mass
711 Spectrometry, Atmos Chem Phys, 10, 4625-4641, DOI 10.5194/acp-10-4625-2010, 2010.
712

713 Nolte, C. G., Appel, K. W., Kelly, J. T., Bhave, P. V., Fahey, K. M., Collett Jr, J. L., Zhang, L.,
714 and Young, J. O.: Evaluation of the Community Multiscale Air Quality (CMAQ) model v5.0
715 against size-resolved measurements of inorganic particle composition across sites in North
716 America, Geosci. Model Dev., 8, 2877-2892, 10.5194/gmd-8-2877-2015, 2015.
717

718 Odum, J. R., Hoffmann, T., Bowman, F., Collins, D., Flagan, R. C., and Seinfeld, J. H.:
719 Gas/Particle Partitioning and Secondary Organic Aerosol Yields, Environ Sci Technol, 30, 2580-
720 2585, 10.1021/es950943+, 1996.
721

722 Paatero, P., and Tapper, U.: Positive Matrix Factorization - a Nonnegative Factor Model with
723 Optimal Utilization of Error-Estimates of Data Values, Environmetrics, 5, 111-126, DOI
724 10.1002/env.3170050203, 1994.
725

726 Palm, B. B., de Sá, S. S., Day, D. A., Campuzano-Jost, P., Hu, W., Seco, R., Sjostedt, S. J., Park,
727 J. H., Guenther, A. B., Kim, S., Brito, J., Wurm, F., Artaxo, P., Thalman, R., Wang, J., Yee, L. D.,
728 Wernis, R., Isaacman-VanWertz, G., Goldstein, A. H., Liu, Y., Springston, S. R., Souza, R.,
729 Newburn, M. K., Alexander, M. L., Martin, S. T., and Jimenez, J. L.: Secondary organic aerosol
730 formation from ambient air in an oxidation flow reactor in central Amazonia, Atmos. Chem. Phys.
731 Discuss., 2017, 1-56, 10.5194/acp-2017-795, 2017.
732

733 Pathak, R. K., Stanier, C. O., Donahue, N. M., and Pandis, S. N.: Ozonolysis of alpha-pinene at
734 atmospherically relevant concentrations: Temperature dependence of aerosol mass fractions
735 (yields), J Geophys Res-Atmos, 112, Artn D03201

736 Doi 10.1029/2006jd007436, 2007.
737

738 Pye, H. O. T., Luecken, D. J., Xu, L., Boyd, C. M., Ng, N. L., Baker, K. R., Ayres, B. R., Bash, J.
739 O., Baumann, K., Carter, W. P. L., Edgerton, E., Fry, J. L., Hutzell, W. T., Schwede, D. B., and
740 Shepson, P. B.: Modeling the Current and Future Roles of Particulate Organic Nitrates in the
741 Southeastern United States, Environ Sci Technol, 49, 14195-14203, 10.1021/acs.est.5b03738,
742 2015.
743

744 Pye, H. O. T., Murphy, B. N., Xu, L., Ng, N. L., Carlton, A. G., Guo, H., Weber, R., Vasilakos,
745 P., Appel, K. W., Budisulistiorini, S. H., Surratt, J. D., Nenes, A., Hu, W., Jimenez, J. L., Isaacman-
746 VanWertz, G., Misztal, P. K., and Goldstein, A. H.: On the implications of aerosol liquid water
747 and phase separation for organic aerosol mass, Atmos. Chem. Phys., 17, 343-369, 10.5194/acp-
748 17-343-2017, 2017.

749

750 Rindelaub, J. D., Borca, C. H., Hostetler, M. A., Slade, J. H., Lipton, M. A., Slipchenko, L. V.,
751 and Shepson, P. B.: The acid-catalyzed hydrolysis of an α-pinene-derived organic nitrate: kinetics,
752 products, reaction mechanisms, and atmospheric impact, Atmos. Chem. Phys., 16, 15425-15432,
753 10.5194/acp-16-15425-2016, 2016.

754

755 Robinson, N. H., Hamilton, J. F., Allan, J. D., Langford, B., Oram, D. E., Chen, Q., Docherty, K.,
756 Farmer, D. K., Jimenez, J. L., Ward, M. W., Hewitt, C. N., Barley, M. H., Jenkin, M. E., Rickard,
757 A. R., Martin, S. T., McFiggans, G., and Coe, H.: Evidence for a significant proportion of
758 Secondary Organic Aerosol from isoprene above a maritime tropical forest, Atmos Chem Phys,
759 11, 1039-1050, DOI 10.5194/acp-11-1039-2011, 2011.

760

761 Saha, P. K., and Grieshop, A. P.: Exploring Divergent Volatility Properties from Yield and
762 Thermodenuder Measurements of Secondary Organic Aerosol from α-Pinene Ozonolysis, Environ
763 Sci Technol, 10.1021/acs.est.6b00303, 2016.

764

765 Sanchez, J., Tanner, D. J., Chen, D., Huey, L. G., and Ng, N. L.: A new technique for the direct
766 detection of HO2 radicals using bromide chemical ionization mass spectrometry (Br-CIMS): initial
767 characterization, Atmos. Meas. Tech., 9, 3851-3861, 10.5194/amt-9-3851-2016, 2016.

768

769 Saunders, S. M., Jenkin, M. E., Derwent, R. G., and Pilling, M. J.: Protocol for the development
770 of the Master Chemical Mechanism, MCM v3 (Part A): tropospheric degradation of non-aromatic
771 volatile organic compounds, Atmos Chem Phys, 3, 161-180, 2003.

772

773 Shilling, J. E., Chen, Q., King, S. M., Rosenoern, T., Kroll, J. H., Worsnop, D. R., McKinney, K.
774 A., and Martin, S. T.: Particle mass yield in secondary organic aerosol formed by the dark
775 ozonolysis of alpha-pinene, Atmos Chem Phys, 8, 2073-2088, 2008.

776

777 Tasoglou, A., and Pandis, S. N.: Formation and chemical aging of secondary organic aerosol
778 during the β-caryophyllene oxidation, Atmos. Chem. Phys., 15, 6035-6046, 10.5194/acp-15-6035-
779 2015, 2015.

780

781 Tuet, W. Y., Chen, Y., Xu, L., Fok, S., Gao, D., Weber, R. J., and Ng, N. L.: Chemical oxidative
782 potential of secondary organic aerosol (SOA) generated from the photooxidation of biogenic and
783 anthropogenic volatile organic compounds, Atmos. Chem. Phys., 17, 839-853, 10.5194/acp-17-
784 839-2017, 2017.

785

786 Ulbrich, I. M., Canagaratna, M. R., Zhang, Q., Worsnop, D. R., and Jimenez, J. L.: Interpretation
787 of organic components from Positive Matrix Factorization of aerosol mass spectrometric data,
788 Atmos. Chem. Phys., 9, 2891-2918, 2009a.

789

790 Ulbrich, I. M., Canagaratna, M. R., Zhang, Q., Worsnop, D. R., and Jimenez, J. L.: Interpretation
791 of organic components from Positive Matrix Factorization of aerosol mass spectrometric data,
792 Atmos. Chem. Phys., 9, 2891-2918, 10.5194/acp-9-2891-2009, 2009b.
793

794 Vaden, T. D., Imre, D., Beránek, J., Shrivastava, M., and Zelenyuk, A.: Evaporation kinetics and
795 phase of laboratory and ambient secondary organic aerosol, Proceedings of the National Academy
796 of Sciences, 108, 2190-2195, 10.1073/pnas.1013391108, 2011.
797

798 Xu, L., Kollman, M. S., Song, C., Shilling, J. E., and Ng, N. L.: Effects of NOx on the Volatility
799 of Secondary Organic Aerosol from Isoprene Photooxidation, Environ Sci Technol, 48, 2253-2262,
800 10.1021/es404842g, 2014.
801

802 Xu, L., Guo, H., Boyd, C. M., Klein, M., Bougiatioti, A., Cerully, K. M., Hite, J. R., Isaacman-
803 VanWertz, G., Kreisberg, N. M., Knote, C., Olson, K., Koss, A., Goldstein, A. H., Hering, S. V.,
804 de Gouw, J., Baumann, K., Lee, S.-H., Nenes, A., Weber, R. J., and Ng, N. L.: Effects of
805 anthropogenic emissions on aerosol formation from isoprene and monoterpenes in the southeastern
806 United States, Proceedings of the National Academy of Sciences, 112, 37-42,
807 10.1073/pnas.1417609112, 2015a.
808

809 Xu, L., Suresh, S., Guo, H., Weber, R. J., and Ng, N. L.: Aerosol characterization over the
810 southeastern United States using high-resolution aerosol mass spectrometry: spatial and seasonal
811 variation of aerosol composition and sources with a focus on organic nitrates, Atmos. Chem. Phys.,
812 15, 7307-7336, 10.5194/acp-15-7307-2015, 2015b.
813

814 Xu, L., Guo, H., Weber, R. J., and Ng, N. L.: Chemical Characterization of Water-Soluble Organic
815 Aerosol in Contrasting Rural and Urban Environments in the Southeastern United States, Environ
816 Sci Technol, 51, 78-88, 10.1021/acs.est.6b05002, 2017.
817

818 Xu, W., Han, T., Du, W., Wang, Q., Chen, C., Zhao, J., Zhang, Y., Li, J., Fu, P., Wang, Z.,
819 Worsnop, D. R., and Sun, Y.: Effects of Aqueous-Phase and Photochemical Processing on
820 Secondary Organic Aerosol Formation and Evolution in Beijing, China, Environ Sci Technol,
821 10.1021/acs.est.6b04498, 2016.
822

823 Yu, J., Cocker, D. R., Griffin, R. J., Flagan, R. C., and Seinfeld, J. H.: Gas-Phase Ozone Oxidation
824 of Monoterpenes: Gaseous and Particulate Products, J Atmos Chem, 34, 207-258,
825 10.1023/a:1006254930583,
826

827 Yu, L., Smith, J., Laskin, A., Anastasio, C., Laskin, J., and Zhang, Q.: Chemical characterization
828 of SOA formed from aqueous-phase reactions of phenols with the triplet excited state of carbonyl
829 and hydroxyl radical, Atmos. Chem. Phys., 14, 13801-13816, 10.5194/acp-14-13801-2014, 2014.
830

831 Zhang, Q., Jimenez, J. L., Canagaratna, M. R., Ulbrich, I. M., Ng, N. L., Worsnop, D. R., and Sun,
832 Y. L.: Understanding atmospheric organic aerosols via factor analysis of aerosol mass

833   spectrometry: a review, Anal Bioanal Chem, 401, 3045-3067, DOI 10.1007/s00216-011-5355-y,
834   2011.

835

836   Zhang, X., McVay, R. C., Huang, D. D., Dalleska, N. F., Aumont, B., Flagan, R. C., and Seinfeld,
837   J. H.: Formation and evolution of molecular products in α-pinene secondary organic aerosol,
838   Proceedings of the National Academy of Sciences, 112, 14168-14173, 10.1073/pnas.1517742112,
839   2015.

840

841   Zhang, Y., Tang, L., Croteau, P. L., Favez, O., Sun, Y., Canagaratna, M. R., Wang, Z., Couvidat,
842   F., Albinet, A., Zhang, H., Sciare, J., Prévôt, A. S. H., Jayne, J. T., and Worsnop, D. R.: Field
843   characterization of the PM2.5 Aerosol Chemical Speciation Monitor: insights into the composition,
844   sources and processes of fine particles in Eastern China, Atmos. Chem. Phys. Discuss., 2017, 1-
845   52, 10.5194/acp-2017-233, 2017.

846

847

848

849
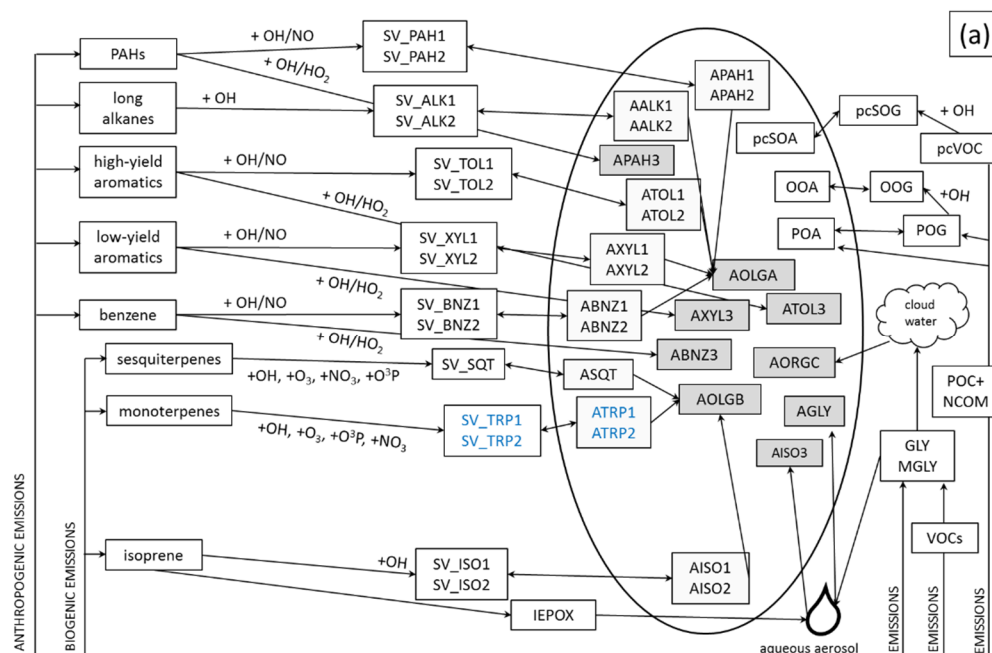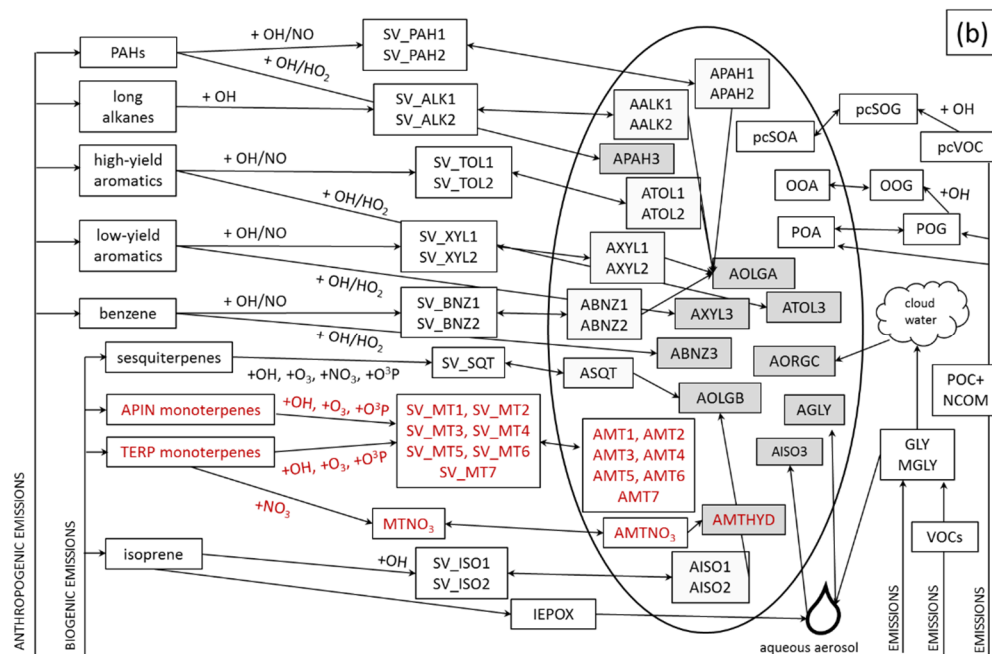
Fig. S1. Schematic of SOA treatment in (a) default simulation and (b) updated simulation in CMAQ. See Pye et al. (2017) for a description of the traditional and aqueous aerosol SOA systems. See Murphy et al. (2017) for a description of the semivolatile POA (POA, POG), oxidized POA vapors (OOA, OOG) and potential SOA from combustion sources (pcSOA) system. See Pye et al. (2015) for MTNO3 formation and hydrolysis. In the default simulation, species in blue were not formed in the updated simulation. In the updated simulation, species in red are different from the default simulation.

857

858
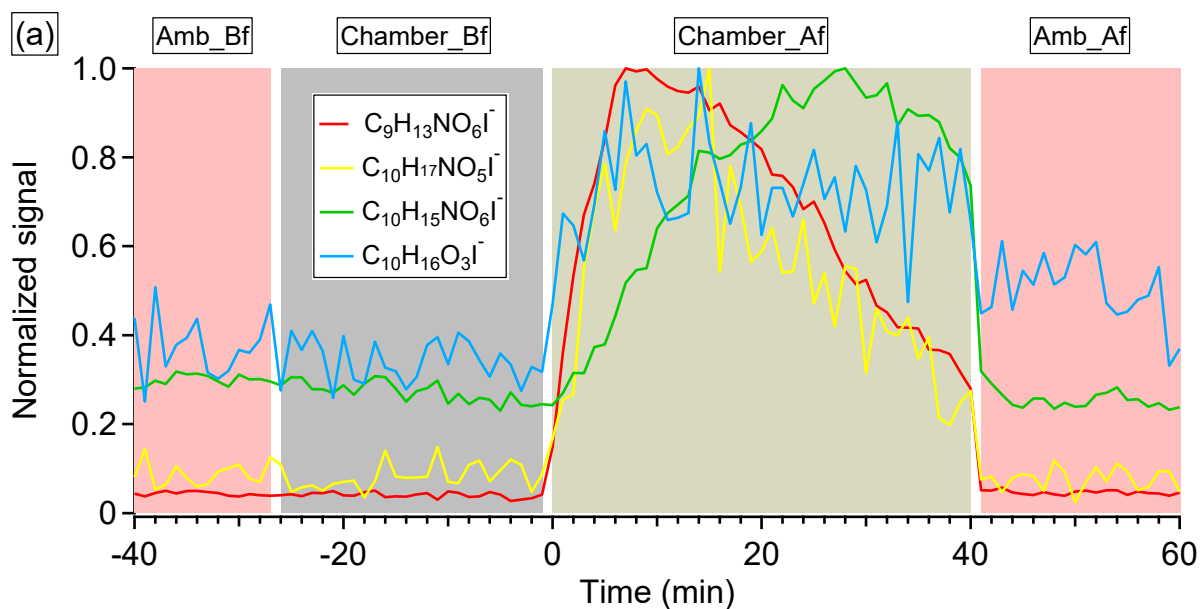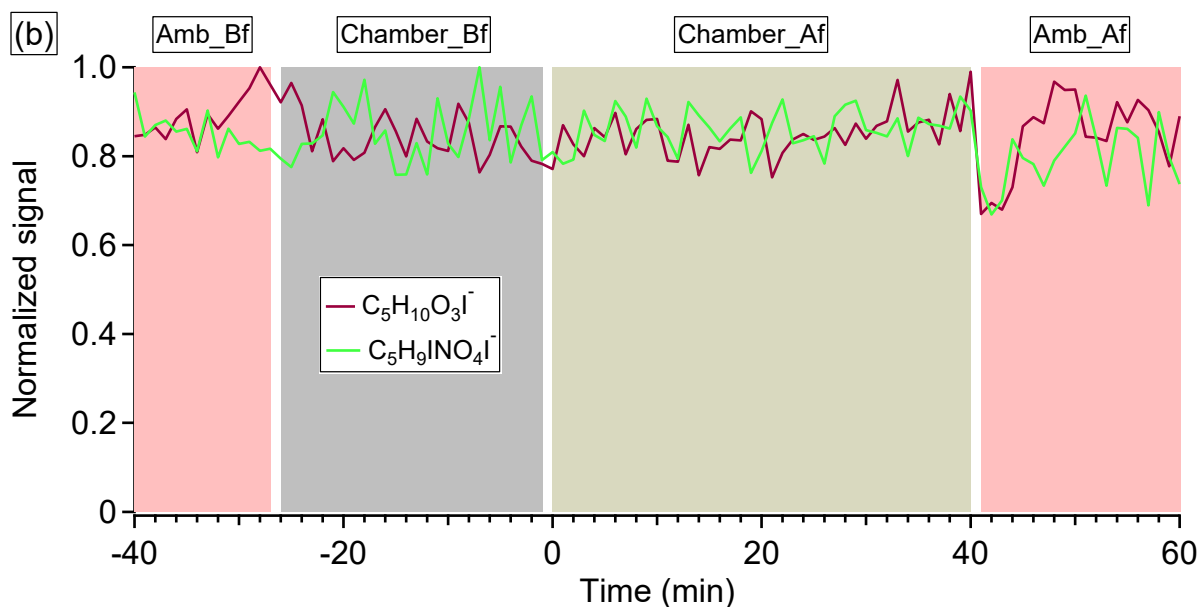
Fig. S2. Time series of gas-phase species detected by HR-ToF-CIMS using I⁻ as reagent ion in experiment ap_0718_1. Panel (a) includes four major known α-pinene oxidation products. Panel (b) includes two major known isoprene oxidation products. The signal is normalized to I⁻ and then normalized to the maximum signal in the time window shown in the figure.

863

864

865
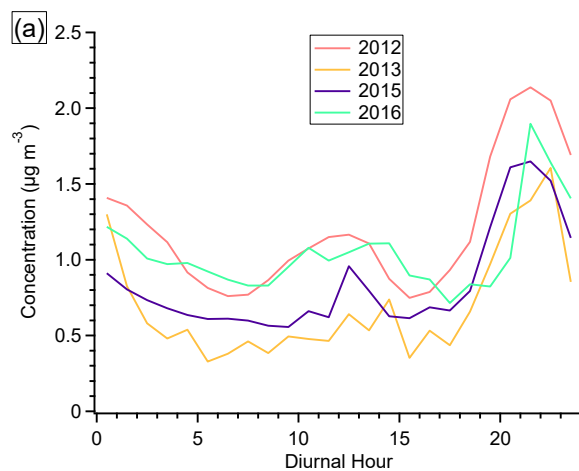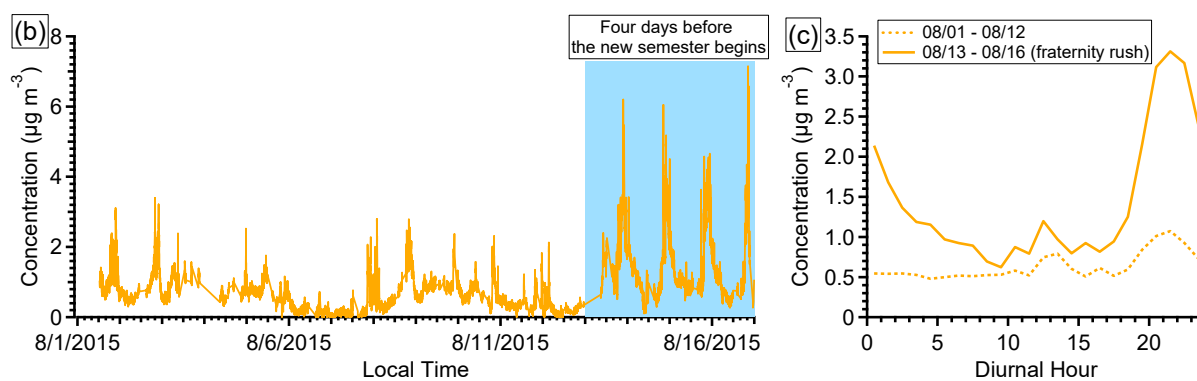
Fig. S3. (a) The diurnal trends of COA in ambient measurements conducted in different years (2012 to 2016). (b) Time series of COA in 2015 measurements. (c) Diurnal trends of COA during two periods of measurements in 2015 (08/01-08/21 and 08/13-08/16).

869
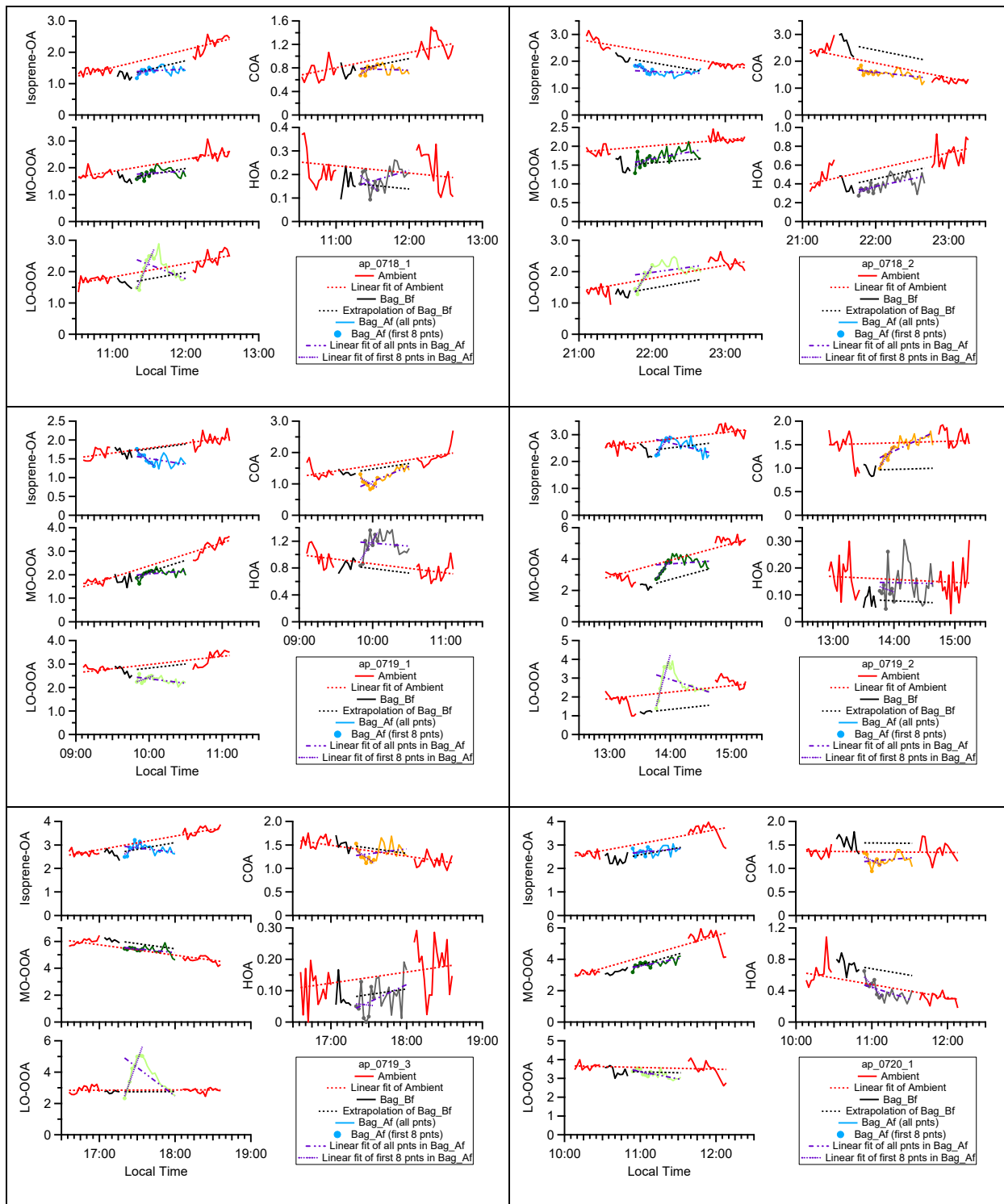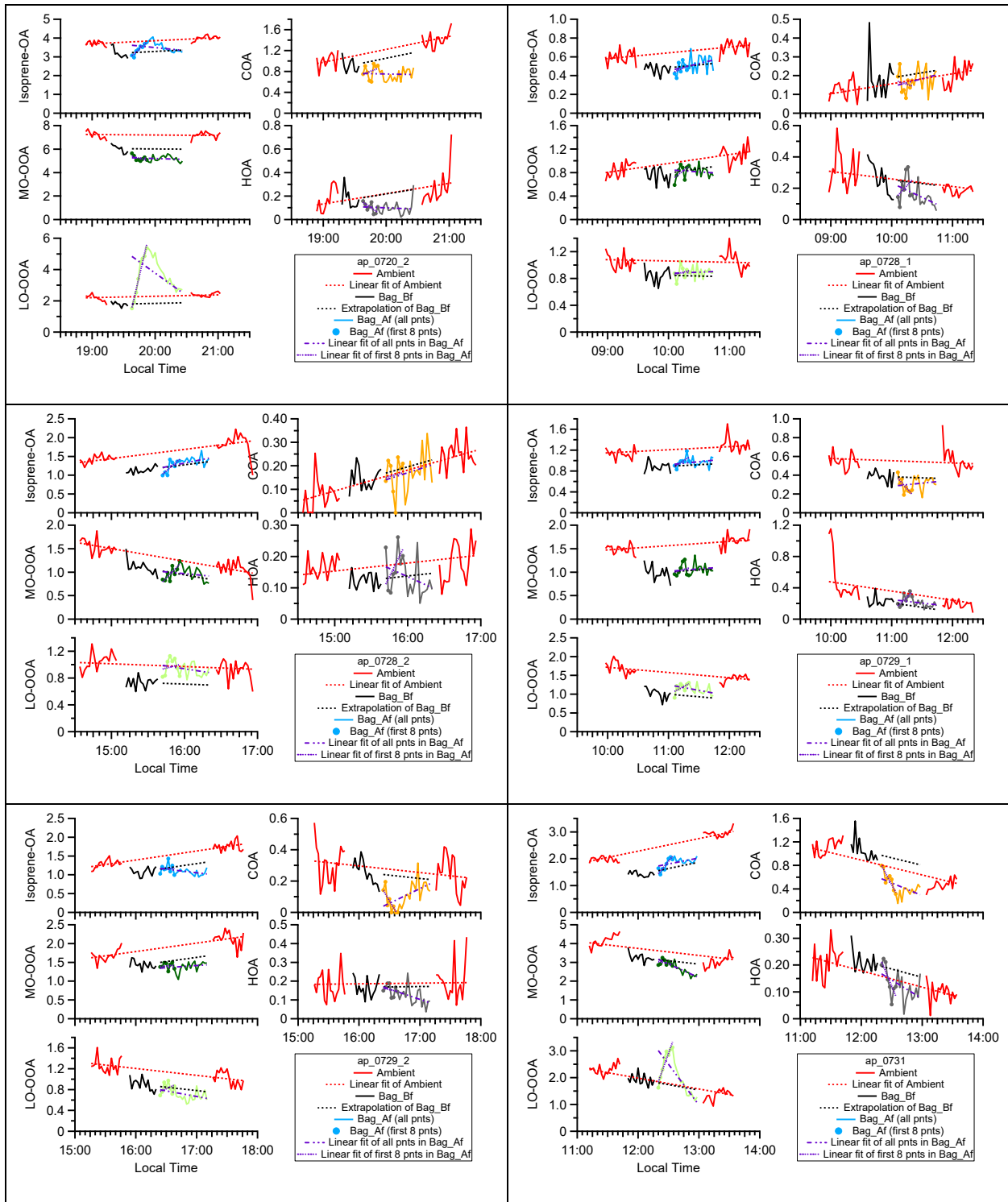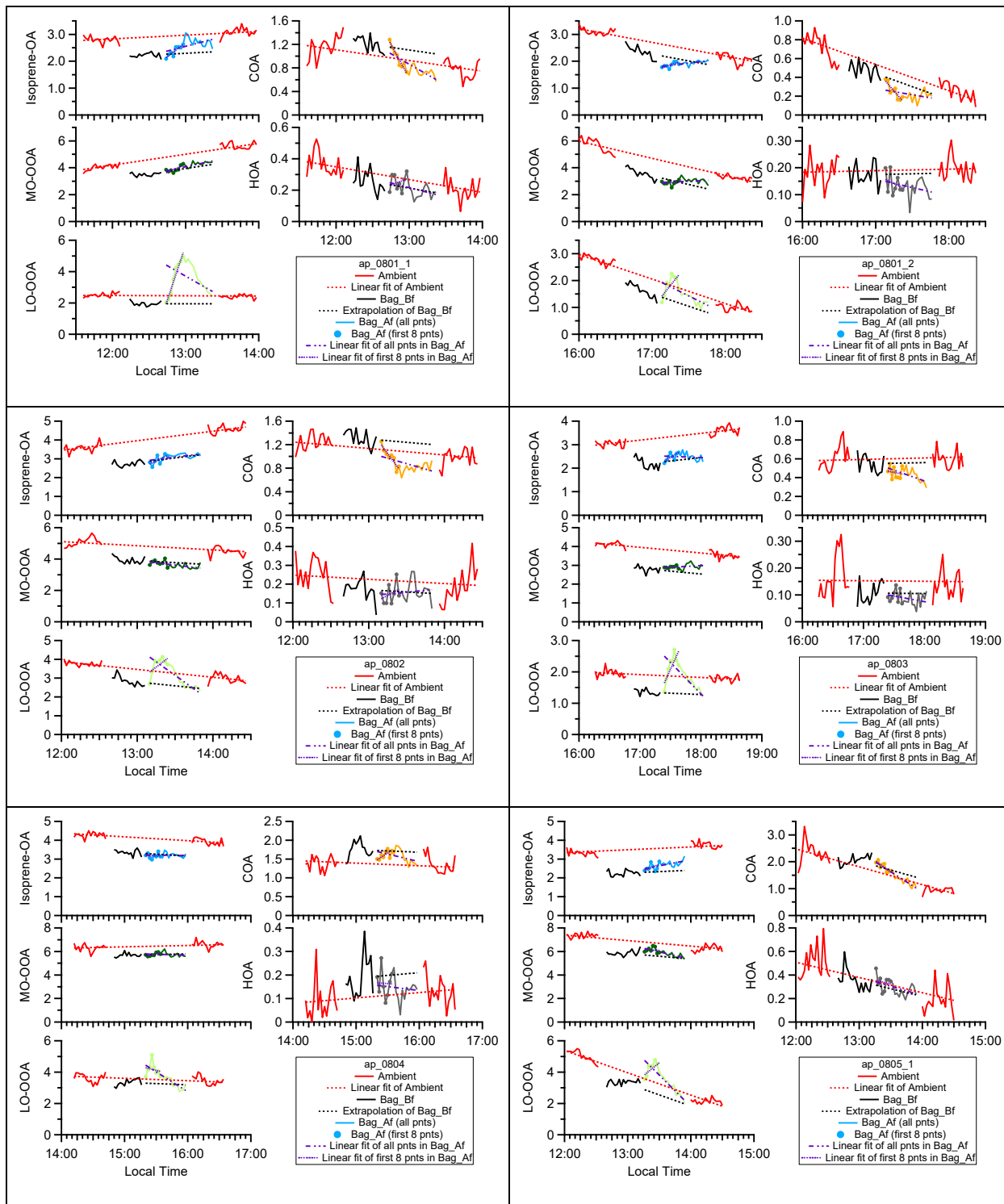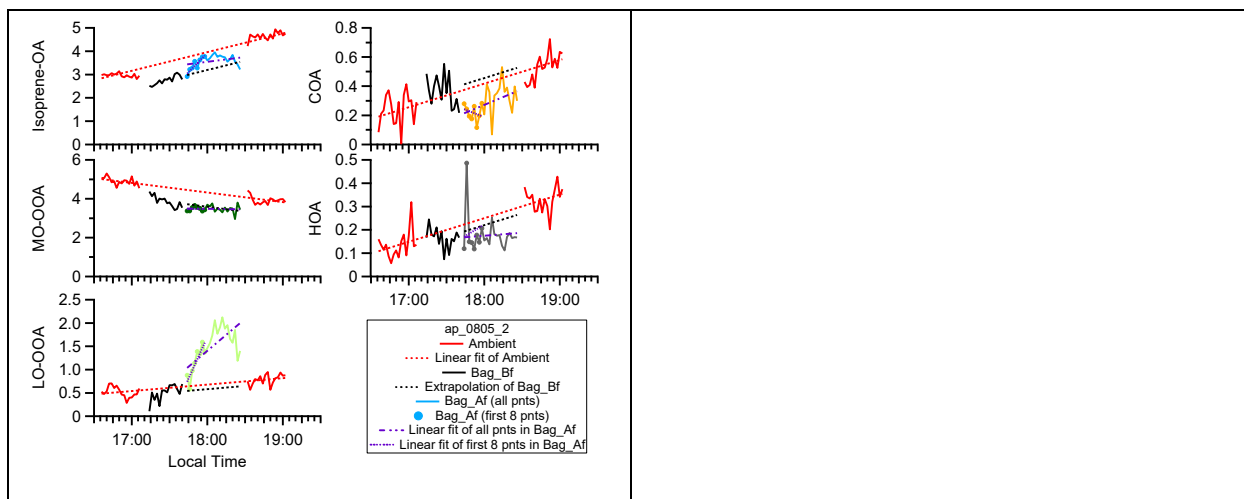
Fig. S4(a). Time series of OA factors in each α-pinene experiment.
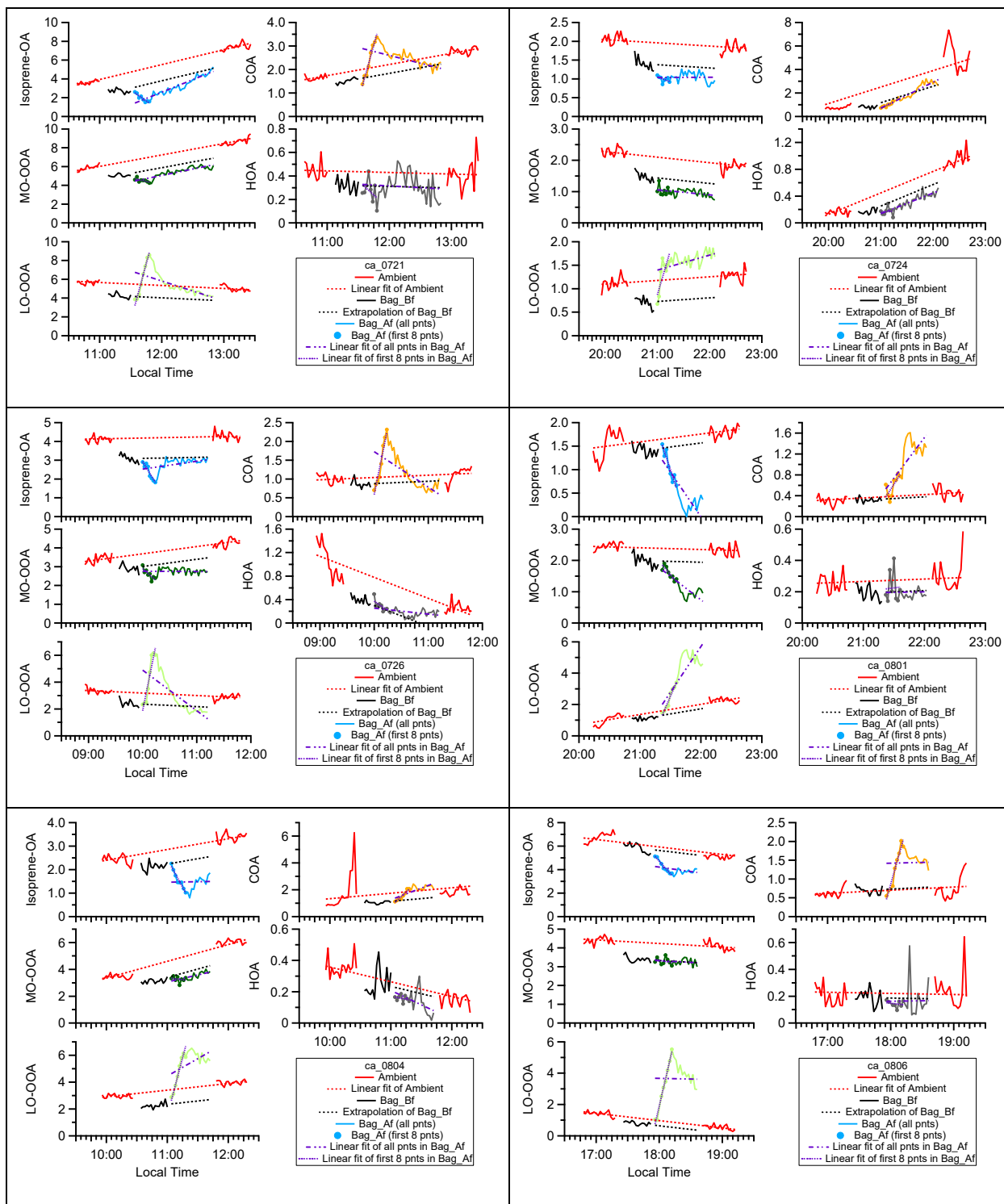
890   Fig. S4(b). Time series of OA factors in each β-caryophyllene experiment.

891

892
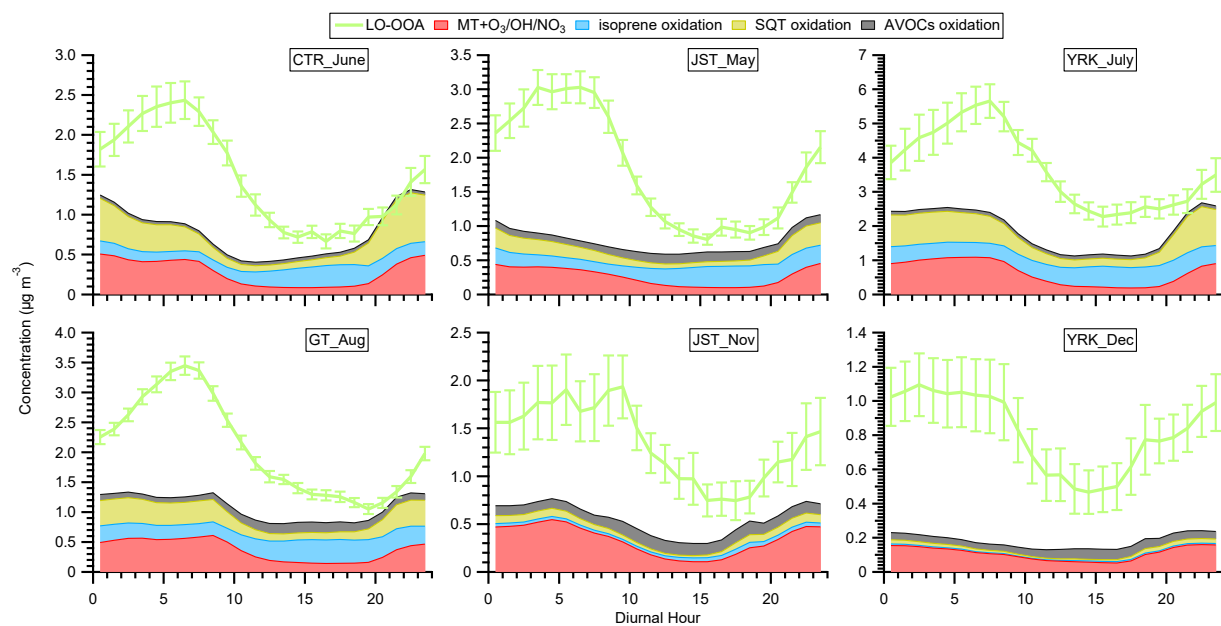
Fig. S5. The diurnal trends of LO-OOA and all fresh SOA (including isoprene (Odum two-product representation), monoterpenes, sesquiterpenes, and anthropogenic VOCs) at different sampling sites in the southeastern U.S. in the default simulation. The error bars indicate the standard error.

896

897
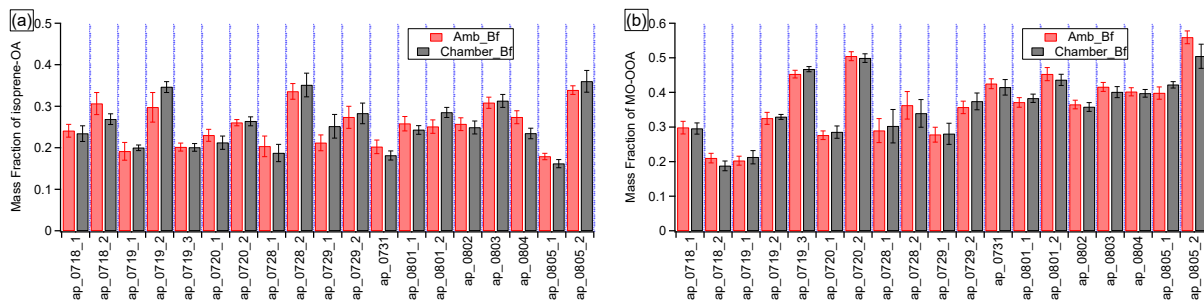
898
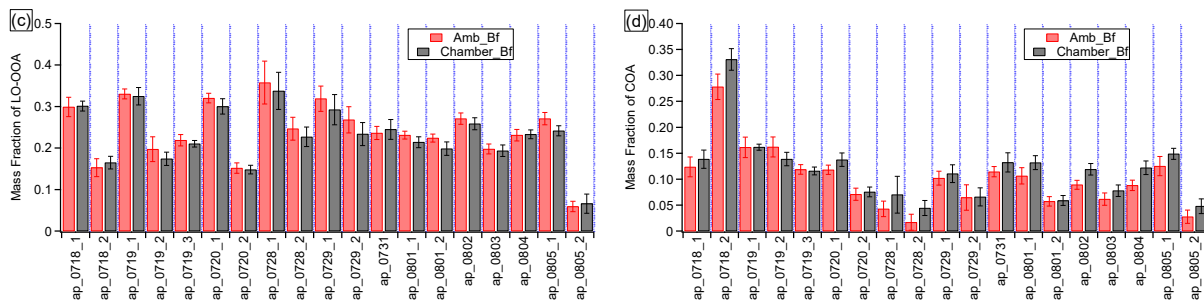
899
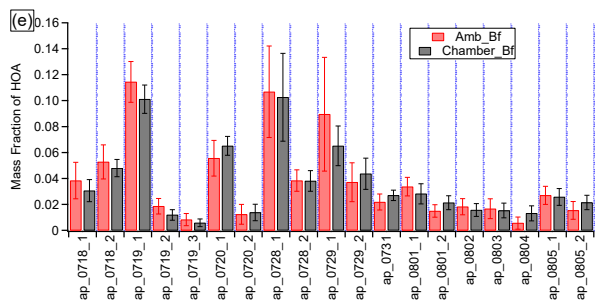
900   Fig. S6. The average mass fraction of OA factors in Amb_Bf and Chamber_Bf periods in α-pinene

901   experiments. The error bars represent the standard deviation. For most experiments, the average

902   mass fractions in these two periods are not statistically significantly different, suggesting that the

903   overall OA compositions are not statistically significantly different between two periods.

904
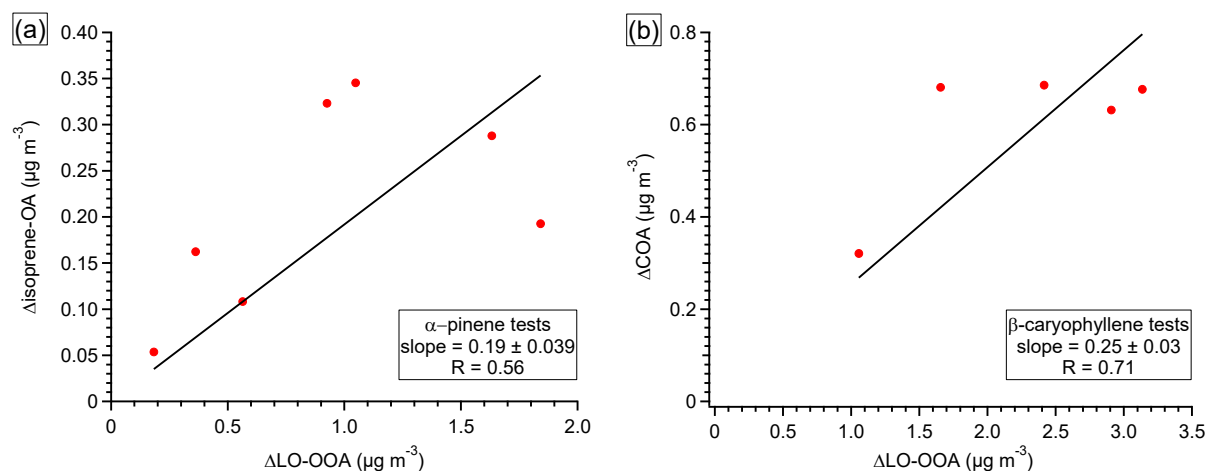
Fig. S7. (a) The relationship between isoprene-OA enhancement and LO-OOA enhancement in α-pinene perturbation experiments. (b) The relationship between COA enhancement and LO-OOA enhancement in β-caryophyllene perturbation experiments. The slopes are from orthogonal fit. The R is from least square fit. The intercepts are forced to be zero. In α-pinene experiments, isoprene-OA enhancement is 19% of LO-OOA enhancement. Thus, every 1 μg m^{-3} SOA is formed from α-pinene oxidation, 0.16 μg m^{-3} [i.e., 0.19/(1+0.19)] is apportioned into isoprene-OA factor and the rest to LO-OOA factor.
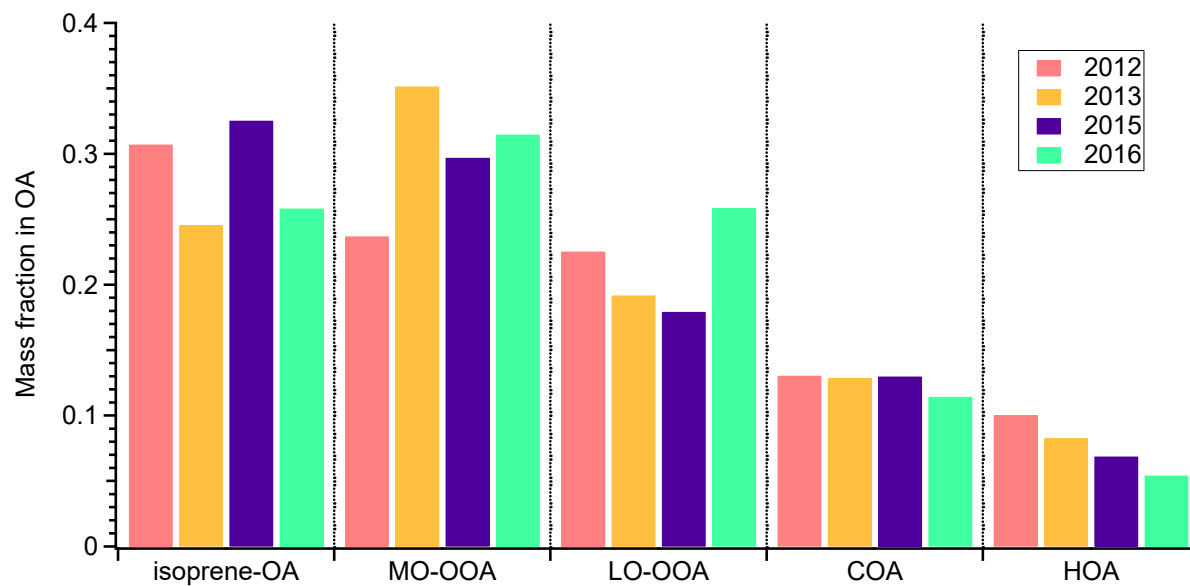
914

915 Fig. S8. The mass fraction of OA factors in ambient measurements conducted in different years

916 (2012 to 2016).

917
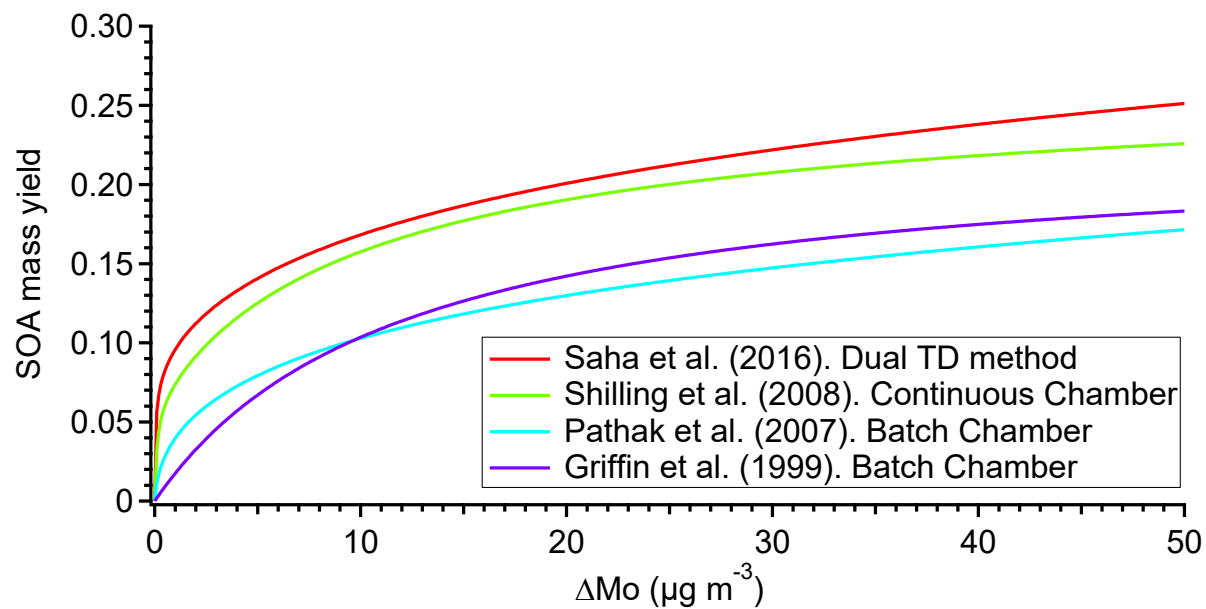
918

919　Fig. S9. Comparison of the SOA mass yields of α-pinene ozonolysis in the literature. SOA density

920　of 1 g cm^{-3} is used in all studies to facilitate comparison. Note that in Saha et al. (2016), the SOA

921　concentration is required to calculate the SOA yield parameterizations. The yields with 445 μg m^{-}

922　^{3} aerosol loading (column i of Table 1 in Saha et al.) are reported in this study.

923
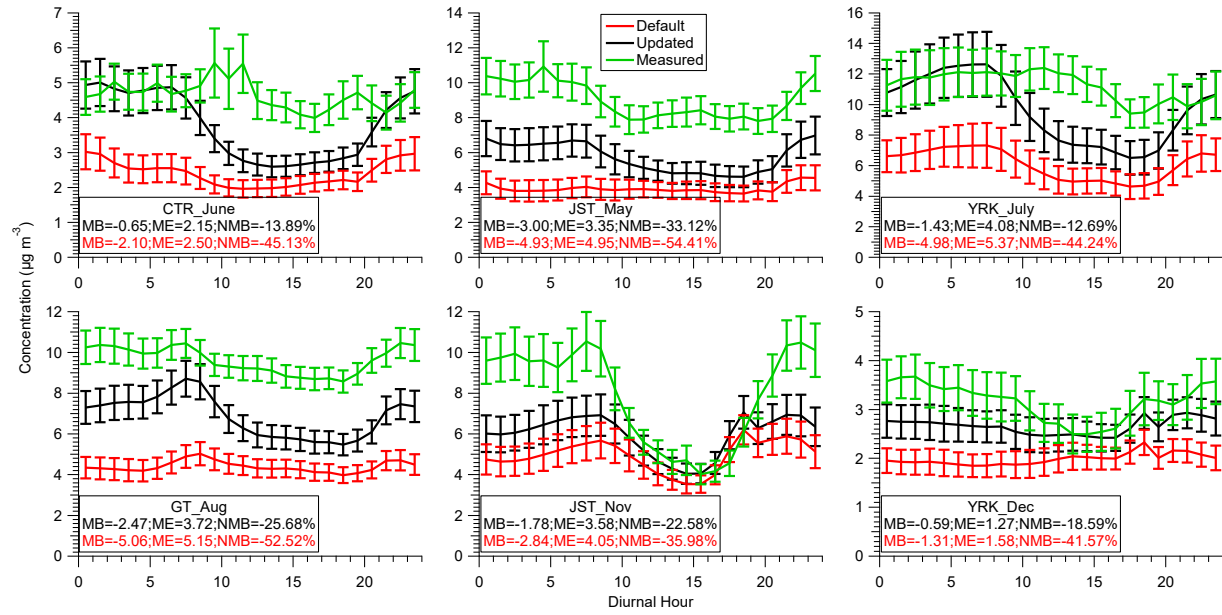
924

925   Fig. S10. The diurnal trends of AMS measured OA and CMAQ predicted OA mass concentration

926   (PM_1) in both default and updated simulations. Mean bias (MB), mean error (ME), normalized

927   mean bias (NMB) are shown in each panel.

928
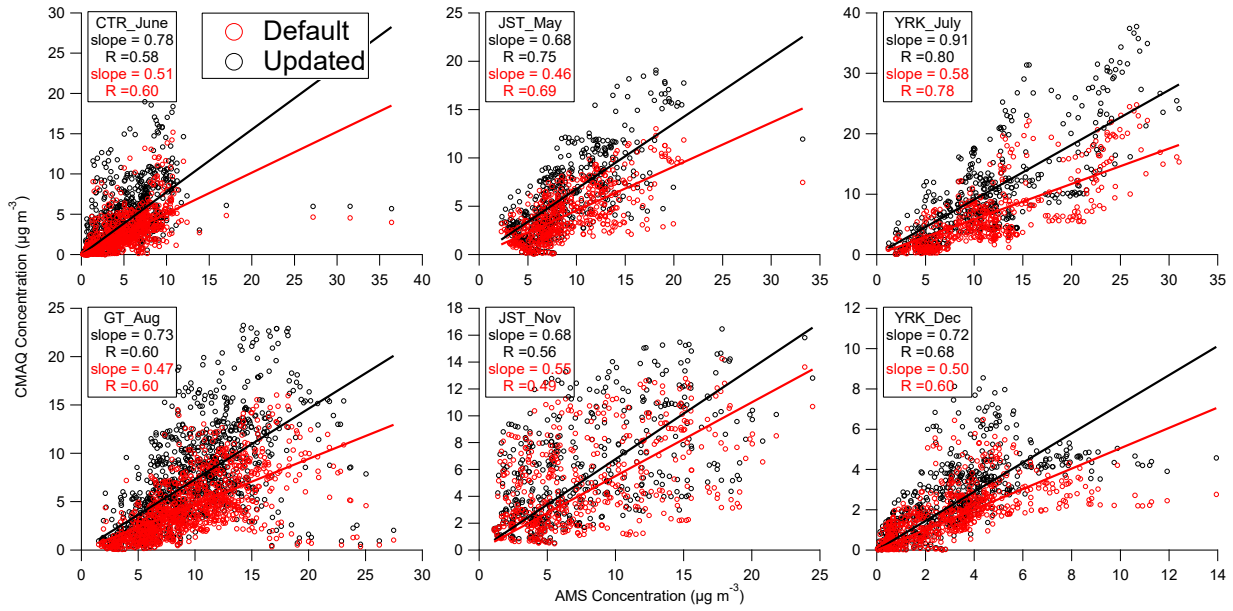
929

930 Fig. S11. The scatter plots of AMS measured OA and CMAQ predicted OA mass concentration in

931 both default and updated simulations. The slopes and R are obtained by least square fit.

932

933
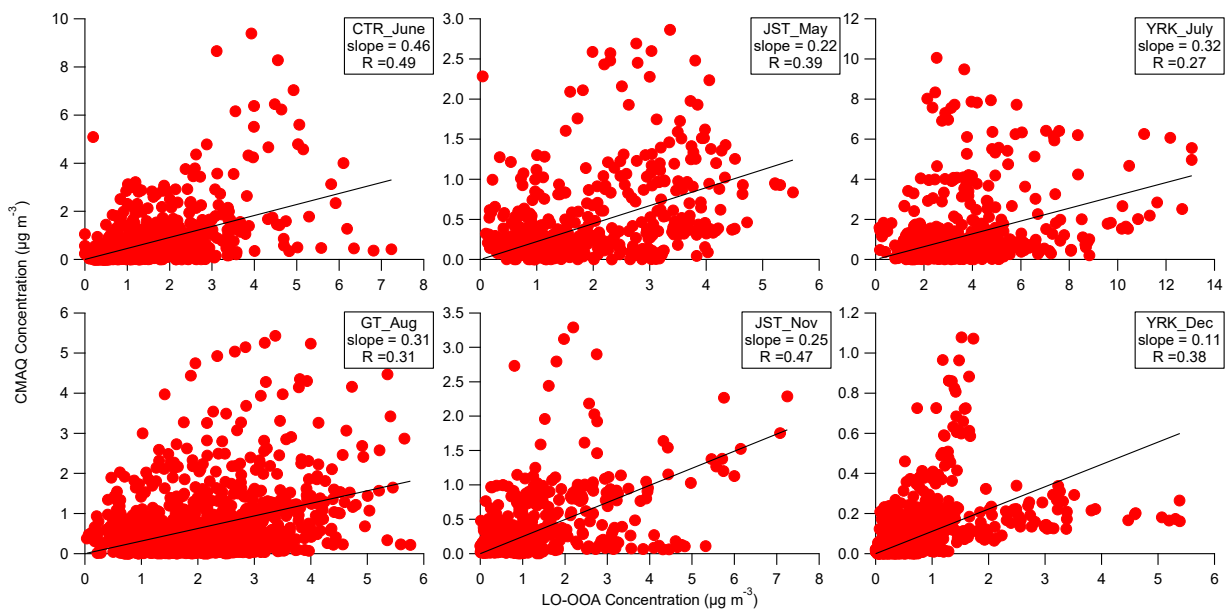
Fig. S12. The scatter plots of LO-OOA and CMAQ predicted SOA mass concentration from monoterpenes and sesquiterpenes in the default simulation at different sampling sites in the southeastern U.S. The slopes and R are obtained by least square fit. The intercepts are forced to be zero.

934
935
936
937

938
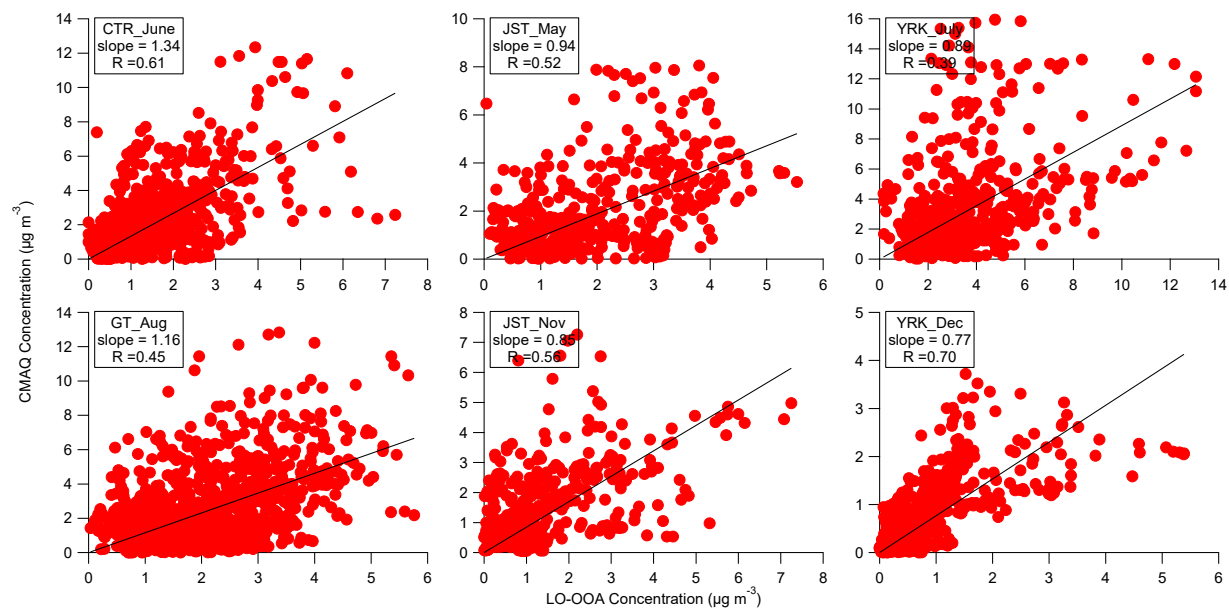
Fig. S13. The scatter plot between LO-OOA and modeled SOA mass concentration from monoterpenes and sesquiterpenes in updated simulation at different sampling sites in the southeastern U.S. The slope sand R are obtained from the least square fit. The intercepts are forced to be zero.

945
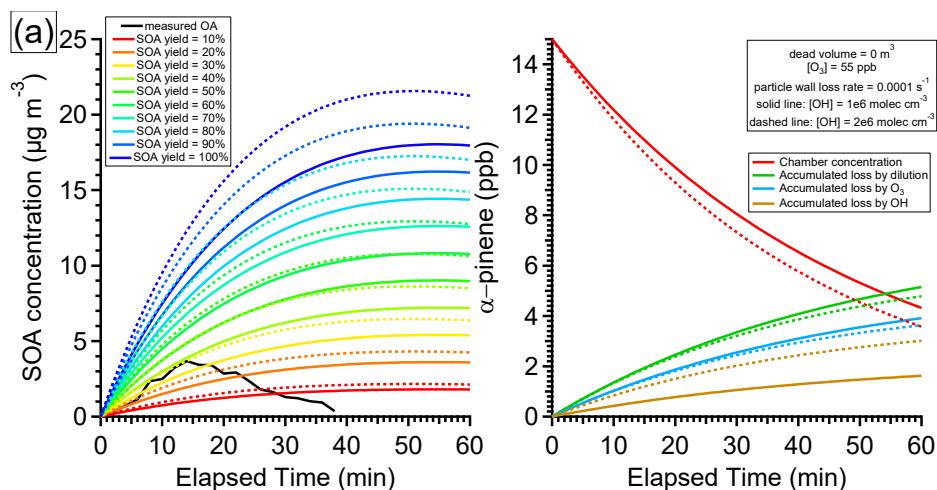
946
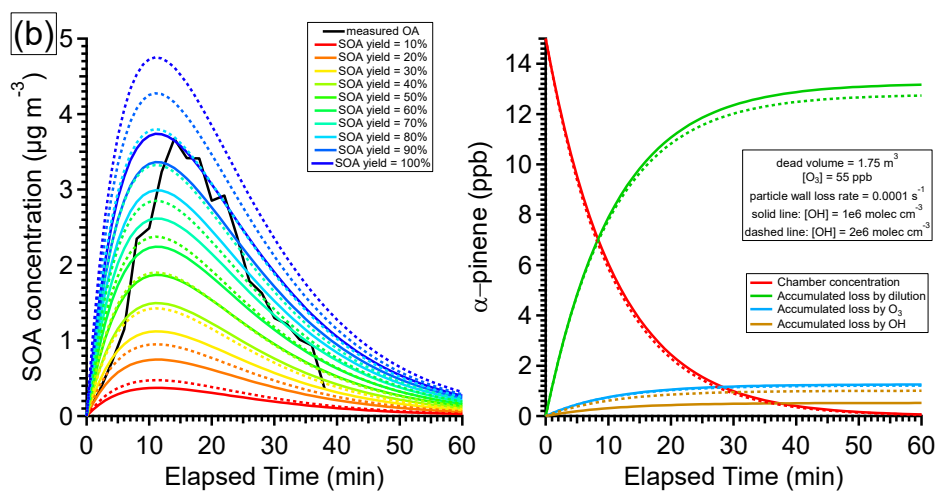
947
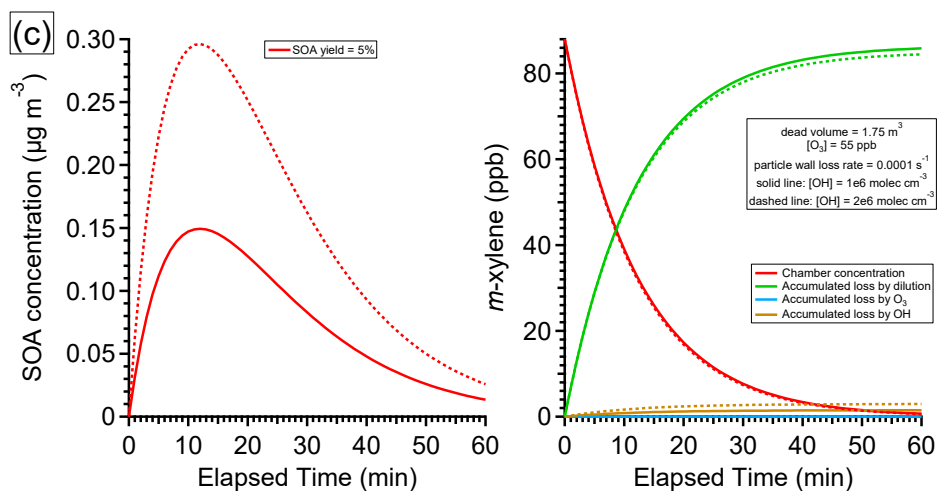
948   Fig. S14. Simulated time series of VOCs and SOA based on a simple box model. (a) α-pinene

949   experiments assuming a range of SOA yields and no dead volume. (b) α-pinene experiments

950   assuming a range of SOA yields and 1.75 m³ dead volume. (c) *m*-xylene experiments assuming 5%

951   SOA yield and 1.75 m³ dead volume.

952

953

954
955
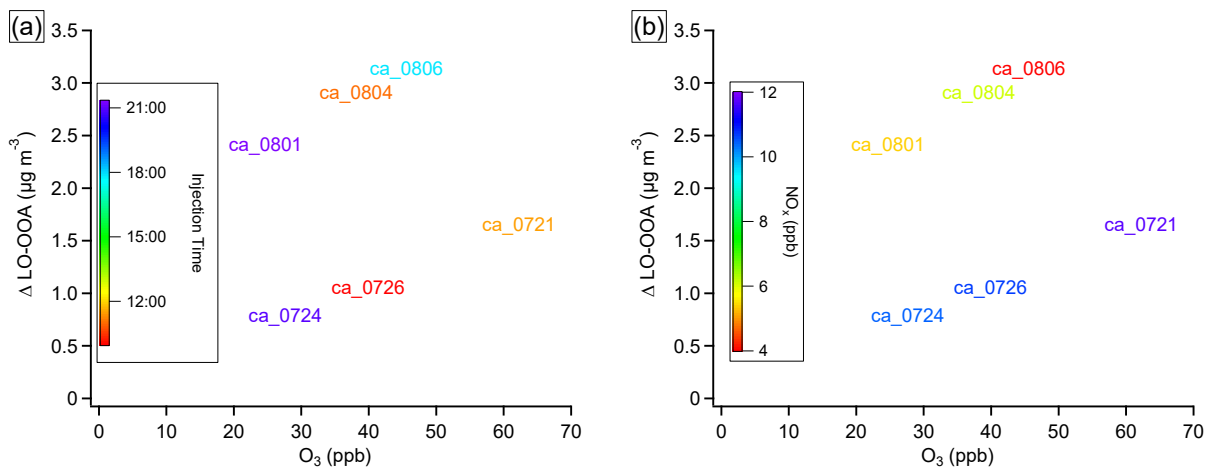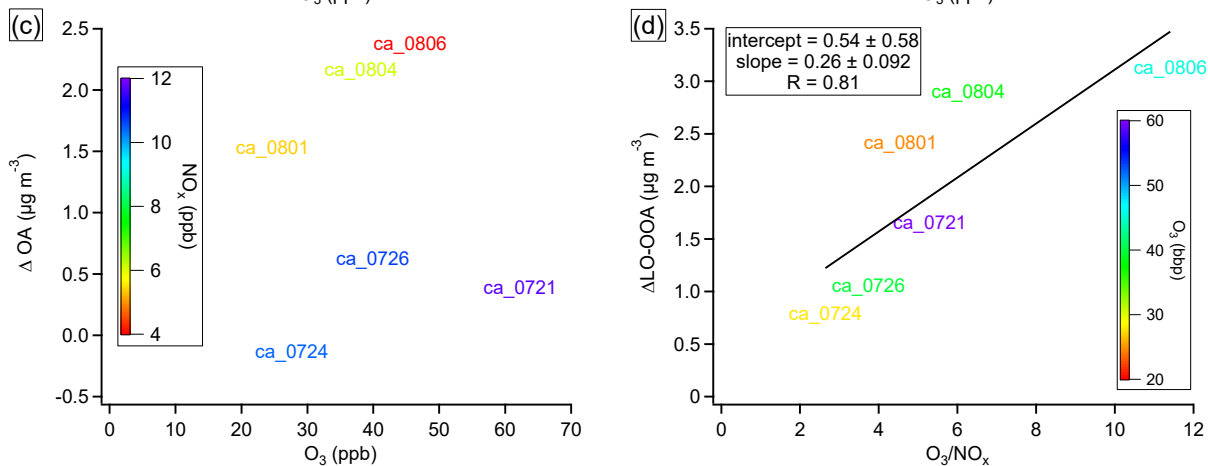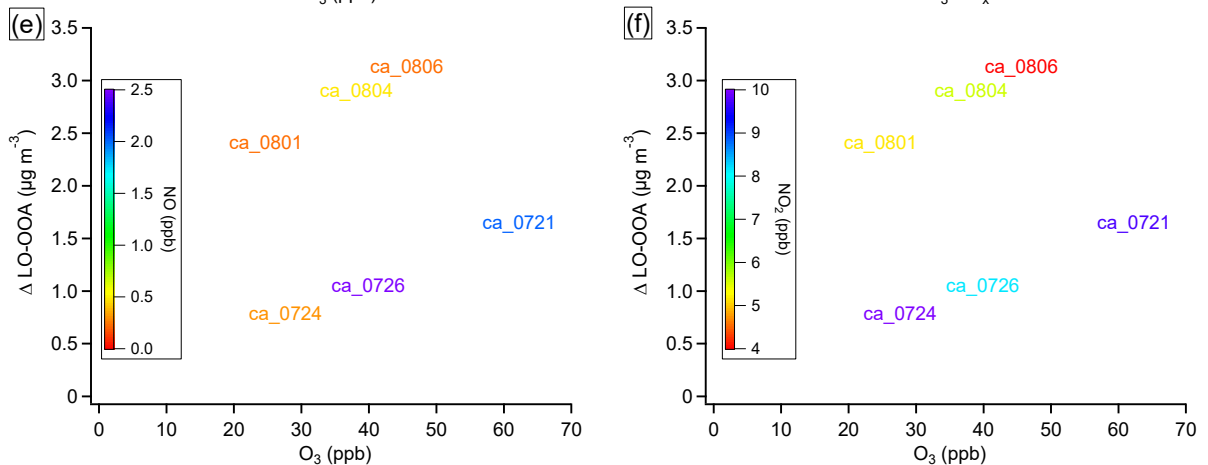
Fig. S15. The influence of NO_x on β-caryophyllene SOA formation. (a) ΔLO-OOA as a function

of O_3, colored by injection time. (b) ΔLO-OOA as a function of O_3, colored by NO_x. (c) ΔOA as

a function of O_3, colored by injection time. (d) ΔLO-OOA as a function of O_3/NO_x ratio, colored

by O_3. The slopes and intercepts are obtained by least square fit. (e) ΔLO-OOA as a function of

O_3, colored by NO. (f) ΔLO-OOA as a function of O_3, colored by NO_2.

961   Table S1. Sampling sites and periods for the Southeastern Center for Air Pollution and

962   Epidemiology (SCAPE) study and the Southern Oxidant and Aerosol Study (SOAS).

963

Site (Abbreviation)	Sampling Period
Jefferson Street (JST_May)	5/10/2012 - 6/2/2012
Yorkville (YRK_July)	6/26/2012 - 7/20/2012
Georgia Tech (GT_Aug)	7/20/2012 - 9/4/2012
Jefferson Street (JST_Nov)	11/6/2012 - 12/4/2012
Yorkville (YRK_Dec)	12/5/2012 - 1/10/2013
Centreville (CTR_June)	6/1/2013 – 7/15/2013

964

965

966

967

968

969

970

971

972   Table S2. The experimental conditions of laboratory α-pinene experiments.

Expt.	[HC]$_0$ (ppb)	Oxidant precursor	RH	NO (ppb)[b]	NO$_2$ (ppb)[b]	O$_3$ (ppb)[b]	OH (10^6 molec cm^{-3})[e]
1	334[a]	H$_2$O$_2$	40%	<DL, <DL[c]	<1, <1[c]	N.A.	1.0
2	174[a]	HONO	<5%	269, 167	310, 440	5, 32	10.9
3	15	NO$_2$	50%	23, 7[d]	60, 60	20, 71	3.6

973   [a]More than 100ppb α-pinene is injected in the first two experiments. It is because these two

974   experiments were designed to produce large amounts of SOA for filter collection and offline

975   analysis.

976   [b]There are two values in these columns. The first value represents the initial concentration when

977   turning on the lights. The second value represents the concentration when the OA concentration

978   reaches about 10 µg m^{-3}.

979   [c]Background NO$_x$ level in the chamber.

980   [d]The initial concentrations of NO, NO$_2$, and O$_3$ in NO$_2$+hν experiments are reported at 3 min after

981   turning on lights.

982   [e]The OH concentration is estimated based on the decay of α-pinene, after considering the

983   consumption of α-pinene by O$_3$.

984

Table S3. The properties of the lumped oxidation products from monoterpenes + O_3/OH.

Species	α[1]	C*[1]	enthalpy[1]	Potential surrogate structure	nC[2]	nO[2]	nH[2]	MW	OM/OC	H[3]	V lebas	Dg	density
	g g⁻¹	μg m⁻³	kJ mol⁻¹					g mol⁻¹	g g⁻¹	M atm⁻¹	cm³ mol⁻¹	cm² s⁻¹	g cm⁻³
MT1	0.040	0.01	102.0	$C_{15}H_{24}O_6$ (Zhang et al., 2015)	15	6	24	300	1.67	7.1E+11	355.2	0.0424	1.4
MT2	0.032	0.1	91.0	$C_{10}H_{16}O_4$ (Chan et al., 2009; Zhang et al., 2015)	10	4	16	200	1.67	8.9E+10	236.8	0.0556	1.4
MT3	0.032	1	80.0	pinic acid (Yu et al.)	9	4	14	186	1.72	1.1E+10	214.6	0.0583	1.4
MT4	0.103	10	69.0	hydroxypinonaldehyde (Yu et al.)	10	3	16	184	1.53	1.4E+09	229.4	0.0587	1.4
MT5	0.143	100	58.0	norpinonic acid (Yu et al.)	9	3	14	170	1.57	1.8E+08	207.2	0.0619	1.4
MT6	0.285	1000	47.0	pinonaldehyde (Yu et al.)	10	2	16	168	1.40	2.2E+07	222.0	0.0624	1.4
MT7	0.160	10000	36.0	norpinonaldehyde (Yu et al.)	9	2	14	154	1.43	2.8E+06	199.8	0.0661	1.4

[1]α, C* (@298K), and enthalpies are based on TD fit in Table 1 of Saha et al. (2016)(Saha and Grieshop, 2016) assuming an OA concentration of 445 μg m⁻³.

[2]Number of oxygen per surrogate is based on Donahue et al. (2011)(Donahue et al., 2011) relationship as used in Pye et al. (2017)(Pye et al., 2017). Number of carbon and oxygen used to find potential surrogate structure.

[3]Henry's Law Coefficients (H) is based on Hodzic et al. (2014)(Hodzic et al., 2014) and relationship with C*. An enthalpy of solvation of 50 kJ mol⁻¹ is used.

994   Table S4. Experimental conditions for ambient perturbation experiments.

Perturbation	Expt ID[a]	Date	Injection Time	Perturbation Amount[b]	NO[c] (ppb)	NO$_2$[c] (ppb)	O$_3$[c] (ppb)
α-pinene	ap_0718_1	7/18/2016	11:18	14	0.69	3.57	48.3
	ap_0718_2	7/18/2016	21:44	14	0.29	10.12	40.2
	ap_0719_1	7/19/2016	9:48	14	7.98	19.96	31.9
	ap_0719_2	7/19/2016	13:44	14	0.46	4.14	71.6
	ap_0719_3	7/19/2016	17:18	14	0.19	4.29	81.9
	ap_0720_1	7/20/2016	10:52	14	1.96	9.09	56.5
	ap_0720_2	7/20/2016	19:36	14	0.10	3.54	75.0
	ap_0728_1	7/28/2016	10:04	14	1.53	3.97	25.3
	ap_0728_2	7/28/2016	15:40	14	0.75	3.12	32.7
	ap_0729_1	7/29/2016	11:04	14	1.55	5.69	36.8
	ap_0729_2	7/29/2016	16:22	14	0.63	3.61	43.6
	ap_0731	7/31/2016	12:18	14	0.19	2.73	48.5
	ap_0801_1	8/1/2016	12:42	14	0.24	5.28	53.1
	ap_0801_2	8/1/2016	17:06	14	0.25	3.23	44.9
	ap_0802	8/2/2016	13:08	14	0.23	3.41	48.5
	ap_0803	8/3/2016	17:22	14	0.14	2.65	53.2
	ap_0804	8/4/2016	15:18	14	0.27	6.04	53.2
	ap_0805_1	8/5/2016	13:14	14	0.27	6.02	60.5
	ap_0805_2	8/5/2016	17:42	28	0.13	3.13	52.4
β-caryophyllene	ca_0721	7/21/2016	11:32	10	2.02	9.73	62.3
	ca_0724	7/24/2016	20:58	10	0.32	10.12	27.6
	ca_0726	7/26/2016	9:58	10	2.48	8.19	39.9
	ca_0801	8/1/2016	21:20	10	0.24	5.19	24.7
	ca_0804	8/4/2016	11:02	10	0.48	5.60	38.1
	ca_0806	8/6/2016	17:54	10	0.23	3.77	45.6

995   [a]Expt ID is named as "perturbation species + date + experiment number". For example, ap_0801_1
996   represents the first α-pinene perturbation experiment on 08/01.

997   [b]The unit for the perturbation in α-pinene and β-caryophyllene experiments is ppb. The
998   perturbation amounts of α-pinene and β-caryophyllene are estimated based on the VOC injection
999   volume and chamber volume. The amount of VOC injected is not the same as the amounts
1000   consumed by oxidants (section S6).

1001   [c]Average concentration during the Chamber_Af period.

1002

1003

1004

1005

1006   Table S5. Sampling periods for the measurements at the GT site from 2012 to 2016.

Year	Sampling Period	Note	Reference
2012	7/21 - 9/3	Continuously ambient measurements	Xu et al. 2015 ACP
2013	8/1/- 8/25	AMS alternates between ambient line and PILS line	Xu et al. 2017 ES&T
2015	8/1 - 8/16	Ambient perturbation experiments and experiments for other purposes	This study
2016	7/1 - 8/6	Ambient perturbation experiments	This study

1007

1008

1009

1010

1011

1012

1013

1014

1015

1016

1017

1018

1019

1020

1021

1022

1023

1024

1025

1026

1027

1028

1029

1030

1031

1032

1033

1034

1035

1036

1037

1038

1039

1040

1041

1042